



High resolution biogenic global emission inventory for the time period 2000-2019 for air quality modelling

Katerina Sindelarova¹, Jana Markova^{1,2}, David Simpson^{3,4}, Peter Huszar¹, Jan Karlicky¹, Sabine Darras⁵, Claire Granier^{6,7}

5

¹Charles University, Faculty of Mathematics and Physics, Dept. of Atmospheric Physics, Prague, Czechia

²Czech Hydrometeorological Institute, Prague, Czechia

³Climate Modelling and Air Pollution Division, Research and Development Dept. Norwegian Meteorological Institute, Oslo, Norway

10 ⁴Dept. Space, Earth & Environment, Chalmers Univ. Tech. Gothenburg, Sweden

⁵Observatoire Midi-Pyrénées, Toulouse, France

⁶Laboratoire d'Aérodynamique, Université de Toulouse, CNRS, UPS, Toulouse, France

⁷NOAA Chemical Sciences Laboratory and CIRES, University of Colorado Boulder, Boulder, Colorado, USA

Correspondence to: Katerina Sindelarova (katerina.sindelarova@mff.cuni.cz)

15 **Abstract.** Biogenic volatile organic compounds (BVOCs) emitted from the terrestrial vegetation into the Earth's atmosphere play an important role in atmospheric chemical processes. A gridded information of their temporal and spatial distribution is therefore needed for proper representation of the atmospheric composition by the air quality models. Here we present three newly developed high-resolution global emission inventories of the main BVOC species including isoprene, monoterpenes, sesquiterpenes, methanol, acetone and ethene. Monthly mean and monthly averaged daily profile emissions were calculated
20 by the Model of Emission of Gases and Aerosols from Nature (MEGANv2.1) driven by meteorological reanalyses of the European Centre for Medium-Range Weather Forecasts for the period of 2000-2019. The dataset CAMS-GLOB-BIOv1.2 is based on ERA-Interim meteorology, datasets CAMS-GLOB-BIOv3.0 and v3.1 were calculated with ERA5. Furthermore, European isoprene emission potential data were updated using high-resolution land cover maps and detailed information of tree species composition and emission factors from the EMEP MSC-W model system. Updated isoprene emissions are
25 included in CAMS-GLOB-BIOv3.1 dataset. The effect of annually changing land cover on BVOC emissions is captured by the CAMS-GLOB-BIOv3.0 as it was calculated with land cover data provided by the Climate Change Initiative of the European Space Agency (ESA-CCI). The global total annual BVOC emissions averaged over the simulated period vary between the datasets from 424 to 591 Tg(C) yr⁻¹, with isoprene emissions from 299.1 to 440.5 Tg(isoprene) yr⁻¹. Differences between the
30 datasets and variation in their emission estimates suggests the emission uncertainty range and the main sources of uncertainty, i.e. meteorological inputs, emission potential data and land cover description. The CAMS-GLOB-BIO time series of isoprene and monoterpenes were compared to other available data. There is a general agreement in an inter-annual variability of the emission estimates and the values fall within the uncertainty range. The CAMS-GLOB-BIO datasets (CAMS-GLOB-BIOv1.2, <https://doi.org/10.24380/t53a-qw03>, Sindelarova et al., 2021a; CAMS-GLOB-BIOv3.0, <https://doi.org/10.24380/xs64-gj42>, Sindelarova et al., 2021b; CAMS-GLOB-BIOv3.1, <https://doi.org/10.24380/cv4p-5f79>, Sindelarova et al., 2021c) are



35 distributed from the Emissions of atmospheric Compounds and Compilation of Ancillary Data (ECCAD) system
(<https://eccad.aeris-data.fr/>, last access: June 2021).

1 Introduction

The biogenic organic volatile compounds (BVOCs) consist of a vast group of non-methane hydrocarbons emitted from
terrestrial vegetation and soils into the Earth's atmosphere (Kesselmeier and Staudt, 1999). They form about 90% of the total
40 atmospheric VOC budget (Guenther et al., 1995) and due to their high reactivity, they are an important component of
atmospheric chemistry (Atkinson and Arey, 2003). Through their oxidation in the atmosphere, BVOCs affect tropospheric
photochemistry and composition (Houweling et al., 1998; Williams et al., 2013).

Their oxidation products play an important role in formation of low-level ozone and secondary organic aerosols thus having
45 impact on air quality and Earth's radiative budget. Their impact on tropospheric ozone levels was evaluated by series of
modelling studies on both global (e.g. Poisson et al., 2000; Pfister et al., 2008) and regional scales (e.g. Curci et al., 2009;
Sartelet et al., 2012; Situ et al., 2013; Tagaris et al., 2014). The evidence of formation of secondary organic aerosols from
BVOC oxidation products was observed by experimental studies (e.g. Griffin et al., 1999; Hao et al., 2011) and field studies
(Lemire et al., 2002; Gelencser et al., 2007; Ehn et al., 2014), and consequently evaluated by atmospheric chemistry models
50 (e.g. van Donkelaar et al., 2007; Simpson et al., 2007; Hodzic et al., 2010; Wu et al., 2020).

The emission of BVOCs from vegetation depends on many environmental factors such as meteorology, especially air
temperature and solar radiation, type of vegetation, seasonal cycle, atmospheric chemistry and composition (Guenther et al.,
1995) and therefore varies significantly in space and time. As biosphere-atmosphere interaction is a very complex system with
55 mutual feedbacks, efforts have been made to assess the impact of different driving factors which themselves are changing
and/or are expected to change in the future. An interest has been focused mainly on impact of changing climate, land cover
and atmospheric CO₂ concentration in the recent past (e.g. Naik et al., 2004; Lathière et al., 2006; Arneth et al., 2007a;
Stavrakou et al., 2014) as well as in the future (e.g. Sanderson et al., 2003; Heald et al., 2008; Hantson et al., 2017).

60 Given the importance of BVOCs in the atmospheric composition, a proper information of amount and spatio-temporal
distribution of BVOC emissions is a crucial input to atmospheric chemistry and climate models. Different ground-based
measurement techniques can be applied to sample BVOC emissions at different scales, from leaf to regional level, as
summarized by Hewitt et al. (2011). Many measurement campaigns have been organized in the past to evaluate BVOC
emission fluxes at different parts of the world, especially in the tropics which have the highest emission potential such as the
65 Amazon (e.g. Rinne et al., 2002; Kuhn et al., 2007; Karl et al., 2007; Eerdekens et al., 2009) and Southeast Asia (e.g. Langford
et al., 2010, Misztal et al., 2011). However, such measurements are unfortunately limited in space and time and are therefore



not fully suitable to create a long-term gridded inventory of BVOC emissions required by the models. Knowledge obtained from observations on the emission processes, speciation and evaluation of fluxes serves as a valuable baseline for development of the emission BVOC models which are then able to simulate BVOC emissions for a specific time period and spatial domain based on defined input parameters.

Over the time a relatively long list of BVOC emission models have been developed. The models differ in used approach to BVOC estimation and level of complexity in considered processes and factors affecting the emission. In general, there are two main approaches to BVOC modelling. First, a so-called *process-based model* that simulates BVOC synthesis directly inside the plant (e.g. LPJ-GUESS, JULES). Second, based on a semi-empirical algorithm described by Guenther et al. (1995) which defines dependence of BVOC emissions from the plant on environmental factors, namely air temperature and solar radiation. From the latter developed the MEGAN model, widely used in the BVOC emission and atmospheric chemical and climate modelling communities. The emission algorithms can either be used as stand-alone, or can be embedded inside an Earth system, land surface or air quality model.

Different BVOC emission models were applied in the past to obtain estimates of BVOC emission levels on global scale (e.g. Lathière et al., 2005; Müller et al., 2008; Arneth et al., 2007b; Schurgers et al., 2009; Pacifico et al., 2011; Guenther et al., 2012; Sindelarova et al., 2014; Messina et al., 2016). Similarly, there exists long list of studies focusing on regional level (e.g. Simpson et al., 1995; Simpson et al., 1999; Steinbrecher et al., 2009; Karl et al., 2009; Oderbolz et al., 2013; Emmerson et al., 2018). These inventories are so called ‘bottom-up’, i.e. calculated by the emission models based on surface input data.

With emerging availability of satellite-based observations of the Earth’s atmosphere, data retrieved from space started to be used also in BVOC emission estimation. Space-borne measurements of suitable chemical species are used to constrain a-priori emissions through an inversion technique applied in the atmospheric chemistry model. Such approach has been applied for example to constrain emissions of isoprene, the most abundant BVOC species, with satellite measurements of isoprene’s oxidation product formaldehyde (e.g. Palmer et al., 2006; Millet et al., 2008; Stavrou et al., 2009; Curci et al., 2010; Bauwens et al., 2016; Kaiser et al., 2018). Emission inventories constrained by satellite observations through application of the model inversion are being called ‘top-down’. Recently, a methodology for direct measurement of isoprene emissions from space has been developed by identifying spectral signatures of isoprene in satellite-borne measurements of Cross-track Infrared Sounder (Fu et al., 2019; Wells et al., 2020).

In this paper we present three new global bottom-up inventories of BVOC emissions calculated with modified version of the state-of-the-art emission model MEGANv2.1 (Guenther et al., 2012) forced by meteorological reanalyzes of the European Centre for Medium-Range Weather Forecasts (ECMWF) and high-resolution input data. The inventories contain global



100 gridded emissions of the main BVOC species for a 20-year period (2000-2019) which can be directly used as an input to the air quality and climate models.

In the following section (Sect. 2) we describe a methodology of emission calculation, including description of the emission model, input meteorological, land cover and emission factor data. Sect. 3 presents global and regional distribution of emission
105 estimates, together with comparison of emission inventories within each other and with other available data. Information on data availability is given in Sect. 4 and conclusions and summary are presented in Sect. 5.

2 Methodology

2.1 Emission model

The presented emission datasets were calculated using the Model of Emissions of Gases and Aerosols from Nature
110 (MEGANv2.1, Guenther et al., 2012). The MEGAN model was developed at the National Center for Atmospheric Research (NCAR, US) and is currently maintained and further improved by Biosphere Atmosphere Interaction Group at University of California – Irvine (<https://bai.ess.uci.edu/>).

It is an emission model extensively used in the atmospheric modelling community for simulation of biogenic VOC emissions
115 from vegetation and soils at regional and global scales (e.g. Guenther et al., 2006; Heald et al., 2008; Arneth et al., 2011; Sindelarova et al., 2014; Seco et al., 2015; Emmerson et al., 2018; Kaiser et al., 2018, Huszar et al, 2018, 2020). Furthermore, the algorithm of the MEGAN model has been embedded into number of Earth system and chemical transport models (e.g. Emmons et al., 2010; Lawrence et al., 2011; Keller et al., 2014; Henrot et al, 2017).

120 The model calculates an emission flux F ($\mu\text{g grid cell}^{-1} \text{ h}^{-1}$) of specific BVOC species from a model grid cell as follows:

$$F = \gamma \cdot EP \cdot S \quad (1)$$

where γ is a dimension-less factor accounting for dependence of emissions on environmental factors (air temperature, solar radiation, ambient CO_2 concentration, leaf age, etc.), EP ($\mu\text{g m}^{-2} \text{ h}^{-1}$) is an emission potential of a grid cell, i.e. a unit emission
125 defined under standardized environmental conditions and S (m^2) is a grid cell surface area. The MEGANv2.1 was applied with the full canopy module which calculates meteorological conditions inside the forest canopy (e.g. leaf temperature, radiation on sunlit and shaded leaves). For calculation of isoprene, the model took into account an inhibitory effect of CO_2 concentration on isoprene emissions using parametrization described in Heald et al. (2009). In our simulations, we did not consider the effect of soil moisture stress on the plant emissions. For more details on the MEGANv2.1 algorithm please see Guenther et al. (2006,
130 2012).



2.2 Meteorology

Two sources of meteorological data were used for calculation of the emission datasets. CAMS-GLOB-BIOv1.2 is based on the ERA-Interim (Dee et al., 2011) data and datasets CAMS-GLOB-BIOv3.0 and v3.1 were calculated with ERA5 (Hersbach et al., 2020), both meteorological reanalyses of the European Centre for Medium-Range Weather Forecasts (ECWMF).
135 MEGAN model requires the following input parameters – 2 m air temperature, water mixing ratio, surface pressure, 10 m wind speed and photosynthetically active radiation (PAR). PAR is defined as solar radiation with wavelength between 400 and 700 nm which photosynthetic organisms are able to absorb during photosynthesis. Unfortunately, this parameter is not available in ERA-Interim nor ERA5 datasets (see Copernicus Knowledge Base – ERA-Interim: surface photosynthetically active radiation (surface PAR) values are too low, 2017). PAR was therefore approximated with surface solar downward radiation divided by
140 a factor of 2.2 as recommended by various studies (Olofsson et al., 2007; Jacovides et al., 2003; Escobedo et al., 2011). The water mixing ratio was calculated from 2 m dew point temperature following equations from Lowe and Ficke (1974).

Since emissions are calculated on a monthly mean basis, the input meteorological data were synoptic monthly means of analyzed and forecasted parameters. ERA-Interim data were available on global grid with horizontal spatial resolution of 0.5°
145 $\times 0.5^\circ$ with 3 or 6 h time steps. The data were linearly interpolated in time in order to obtain monthly averaged daily profile of each meteorological variable. ERA5 is a successor to ERA-Interim with higher horizontal spatial resolution of $0.25^\circ \times 0.25^\circ$ and with 1 h time resolution. Interpolation between time steps was therefore no longer necessary in case of ERA5.

2.3 Vegetation description

The spatial distribution of vegetation in the MEGAN model is defined using plant functional types (PFTs). This is an alternative
150 approach to vegetation description using biomes (e.g. savanna, tundra). While biomes can consist of physiologically distinct vegetation types (e.g. grasses and trees), plant functional types group vegetation with similar leaf physiology. Use of PFTs leads to less complex vegetation representation, but allows physiologically-based ecosystem description convenient for the dynamic global vegetation models. The MEGAN model was designed to be coupled with Community Land model (CLM4) and therefore uses the same approach, i.e. representation of the global land cover with 16 PFT categories (Lawrence and Chase,
155 2007). Vegetation in each model grid cell is defined by fractional coverage by each of the PFT. List of the MEGANv2.1 PFT categories is given in Table 1.

Emissions in CAMS-GLOB-BIOv1.2 and v3.1 were calculated with temporally invariable map of PFTs from CLM4 model representative for the year 2000. However, global land use / land cover is experiencing dramatic changes, e.g. deforestation in
160 the tropical forests and replacement of forests by agricultural land (e.g. Song et al., 2018), which is obviously expected to impact the BVOC emissions. In order to capture the land cover change in MEGAN simulations, we replaced the static CLM4 PFT map with land cover data from the ESA-CCI (ESA, 2017). ESA-CCI data are provided by the Climate Change Initiative



of the European Space Agency. The data consists of time series of global annual mean land cover maps with high horizontal spatial resolution (300 m) available for the period of 1992-2018 based on satellite observations. To be consistent with the MEGAN model, the ESA-CCI land cover categories were converted to PFT classes similar to CLM using the CCI-LC user tool v4.3 (Poulter et al., 2015). Emissions calculated with temporally varying land cover are included in CAMS-GLOB-BIOv3.0 dataset.

Table 1 compares global land areas covered by each PFT category in CLM4 and ESA-CCI (year 2000, converted by CCI-LC user tool) land cover maps. Note that though Corn (Maize) category is included in the MEGAN PFT list, it is currently not distinguished from other crops and its spatial coverage is therefore zero. The two maps differ in the total area covered by vegetation, with ESA-CCI giving ~19% less vegetated area globally. In ESA-CCI, extent of a tree and grass categories is ~25% lower, while coverage by the crop category is almost 50% higher when compared to CLM.

Vegetation seasonality is represented by changes in leaf area index (LAI). LAI is a dimensionless parameter defined as one-sided leaf area per area of the ground surface ($\text{m}^2 \text{m}^{-2}$). Spatial and temporal distribution of LAI was obtained from processed observations of the MODIS instrument (Yuan et al., 2011). The 8-day observations were averaged to monthly means. The Yuan et al. LAI data are available for the period of 2000 – 2016. For the emissions calculated after 2016 a 10-year climatology was used. Since these LAI values represent an average over the whole grid cell, values were divided by a grid cell fraction covered by vegetation to obtain LAI for vegetated area only.

Table 1. List of MEGANv2.1 PFT categories and global coverage by each PFT category (10^6 km^2) according to CLM4 and ESA-CCI (year 2000) land cover maps.

PFT category	global area / 10^6 km^2	
	CLM4	ESA-CCI 2000
Needleleaf evergreen temperate tree	3.63	3.03
Needleleaf deciduous boreal tree	1.48	3.05
Needleleaf evergreen boreal tree	9.92	3.51
Broadleaf evergreen tropical tree	11.83	10.25
Broadleaf evergreen temperate tree	1.91	2.42
Broadleaf deciduous tropical tree	6.13	3.33
Broadleaf deciduous temperate tree	4.63	3.64
Broadleaf deciduous boreal tree	1.76	1.24



Broadleaf evergreen temperate shrub	0.09	1.73
Broadleaf deciduous temperate shrub	5.49	3.09
Broadleaf deciduous boreal shrub	8.18	1.52
Arctic C3 grass	4.31	5.96
Cool C3 grass	12.67	7.97
Warm C4 grass	11.20	6.79
Crops	14.76	21.90
Corn (Maize)	0	0
<i>Total</i>	<i>98.0</i>	<i>79.4</i>

185

2.4 Global emission potential data

Emission potentials are together with the vegetation description a crucial parameter in BVOC emission estimation. In the following text we distinguish between emission factor (EF) and emission potential (EP). By EF we mean emission of a chemical species from specific plant or vegetation type under standard conditions of environmental parameters. EFs can be defined either as area-based values, i.e. an emission from a unit area covered by specific plant or vegetation type (e.g. $\mu\text{g}(\text{species}) \text{m}^{-2} (\text{ground-cover}) \text{h}^{-1}$) or mass-based values, i.e. emission from a unit mass of the plant's dry leaf matter (e.g. $\mu\text{g}(\text{species}) \text{g}^{-1} (\text{dry foliar mass}) \text{h}^{-1}$). With emission potential (EP, $\mu\text{g} \text{m}^{-2} \text{h}^{-1}$) we describe the emission capacity of the whole grid cell which is calculated as a weighted sum of emission factors for all plants or vegetation types present in the grid cell:

195

$$EP = \sum_{veg} f_i EF_i (\mu\text{g} \text{m}^{-2} \text{h}^{-1}) = \sum_{veg} f_i EF_i (\mu\text{g} \text{g}^{-1} \text{h}^{-1}) D_i \quad (2)$$

where f_i is a fraction of a grid cell covered by individual plant or vegetation type and D_i ($\text{g}(\text{dry leaf matter}) \text{m}^{-2}$) is a foliar density of the plant or vegetation type.

200

Emission factors in the MEGANv2.1 model are defined on a canopy-scale level as an emission under standard condition from the full canopy. Above canopy measurements of EF are unfortunately limited, therefore the canopy-scale EFs in MEGAN are still based on leaf- and branch-scale measurements which were extrapolated with a canopy environment model to the canopy level (Guenther et al., 2006). MEGAN standard conditions are defined for series of variables, such as LAI, leaf age composition of the canopy, meteorological conditions (temperature, solar radiation, humidity, wind speed, soil moisture) of the current state and of the past (temperature and solar radiation). For more details see Guenther et al. (2006).

205



210 The MEGAN model has two options for emission potential definition. Either use of the input emission potential maps for selected species or calculation of EP from vegetation coverage. These options are described in more detail in the two following sections.

2.4.1 Emission potentials from detailed global maps

215 The first option consists of the use of annual mean emission potential maps with high spatial resolution for the main BVOC species, i.e. isoprene, main monoterpenes (α -pinene, β -pinene, myrcene, sabinene, limonene, trans- β -ocimene, 3 Δ -carene) and 2-methyl-3-buten-2-ol (MBO). Emission maps are available together with the MEGANv2.1 code (<https://bai.ess.uci.edu/megan/data-and-code/megan21>, access date 31/5/2021) and were created based on detailed ecoregion description, combining information on species composition with species specific emission factors and above canopy flux measurements, where available (Guenther et al., 2012). Emission potentials for the rest of the modeled species were calculated based on the PFT coverage as described in the following section.

2.4.2 Emission potentials calculated from PFTs

220 The second option consists of EP calculation from the vegetation composition of each grid cell. MEGAN uses 16 PFTs for description of vegetation in the model domain (listed in Table 1.). Each of the PFTs is assigned with an emission factor value for each of the modeled species (see Table 2 in Guenther et al., 2012). The emission potential of each grid cell for a specific modeled chemical species is then calculated as a weighted sum defined in Eq. (2).

225 Use of EP calculated from the PFT coverage leads to ~10% decrease of isoprene emission total on global scale when compared to emission calculation based on EP detailed maps. For β -pinene and other monoterpenes the difference is only 1-2 %. However, for α -pinene emissions calculated from PFT coverage are more than 70 % higher when compared to emissions calculated from the EP maps. Therefore, the EFs assigned to each PFT tree category for α -pinene were revised based on recent updates of EFs for the ORCHIDEE model (Messina et al., 2016). The ORCHIDEE and MEGAN models differ in definition of standard conditions which means that the ORCHIDEE EFs needed to be converted to MEGAN suitable format. The conversion was done in a similar way as described in Sect. 2.5.2. The newly used α -pinene EFs are listed in Table 2 together with the original MEGANv2.1 values. The resulting α -pinene emissions calculated with revised EFs are ~ 18% higher than emissions calculated with detailed EP map.

235



Table 2. Updated emission factors for α -pinene ($\mu\text{g m}^{-2} \text{h}^{-1}$) for tree PFT classes used in this study based on Messina et al. (2016) together with original MEGANv2.1 EFs (Guenther et al., 2012).

PFTS	Description	EF α -pinene ($\mu\text{g m}^{-2} \text{h}^{-1}$)	
		this study / Messina et al. (2016)	Guenther et al. (2012)
NT_EG_TEMP	Evergreen needleleaf temperate	373	500
NT_DC_BORL	Deciduous needleleaf boreal	698	510
NT_EG_BORL	Evergreen needleleaf boreal	373	500
BT_EG_TROP	Evergreen broadleaf tropical	386	600
BT_EG_TEMP	Evergreen broadleaf temperate	380	400
BT_DC_TROP	Deciduous broadleaf tropical	386	600
BT_DC_TEMP	Deciduous broadleaf temperate	204	400
BT_DC_BORL	Deciduous broadleaf boreal	259	400

240

Describing global vegetation by only 16 PFT categories is of course a simplification that inevitably brings inaccuracies, especially for categories such as broadleaf deciduous forest which can consist of tree species which are very low isoprene emitters but at the same time tree species such as oaks which are very strong isoprene emitters. On the other hand, such simplifications are often necessary due to lack of detailed information on vegetation composition and/or assignment with emission factor, or is simply a result of balance between the level of detail in vegetation description and ability of the model algorithm to digest such data.

245

Calculation of EP from PFT coverage is to some extent inaccurate, on the other hand allows us to change the land cover description dataset (e.g. use ESA-CCI instead of CLM) and therefore study impact of land cover on resulting emissions.

250 2.5 Update of isoprene emission potentials in Europe

The MEGAN global input emission potential maps for isoprene and main monoterpenes were created based on information of global land cover distribution and vegetation composition in combination with emission factor survey, incorporating results of flux measurement campaigns. Naturally, lot of information on emission factor and flux measurements originates in the tropics as it is a region of the highest emission rates. This leads to the fact that the MEGAN emission potential maps are well suited to for the tropical region, but may be less fitting in other parts of the world.

255

As detailed land cover data were becoming available for Europe, studies focusing on estimation of biogenic VOCs from plant-specific vegetation description started to appear (e.g. Simpson et al., 1995, 1999, Karl et al., 2009; Oderbolz et al., 2013).



260 Several studies have shown large discrepancies between emissions calculated using species-specific emission factors and those calculated by MEGAN-based inputs (Rinne et al., 2009; Langner et al., 2012; Jiang et al., 2019). This motivated us to revise the input emission potential maps for isoprene in this region.

265 In this work, new maps of area-based isoprene emission potentials (EP, $\mu\text{g m}^{-2} \text{h}^{-1}$) for the European area were created. These EP maps are based on detailed maps of forest species and other vegetation combined with Europe-specific emission factors for each species. The EP map update makes use of procedures developed over many years for the EMEP model (Simpson et al., 1995, 1999, 2012). The basic emission factors and LAI changes are taken from a high-resolution version of the EMEP model rv4.33 (Simpson et al., 2012).

270 The EMEP and MEGANv2.1 models differ in their definition of standard environmental conditions for emission factors. In MEGANv2.1 EFs are defined on canopy-scale level, i.e. as an emission from the full canopy, under standardized canopy conditions of LAI, specific proportion of mature, growing and old foliage, current and previous air temperatures and radiation, humidity, wind-speed and soil moisture (Guenther et al., 2006, 2012). The EMEP system, similar to previous BVOC algorithms of Guenther et al. (1995), uses leaf- and branch-level EF definition with standard conditions for leaf temperature (30°C) and photosynthetically active radiation ($1000 \mu\text{mol m}^{-2} \text{s}^{-1}$) only. As canopy-scale EFs are not available for the 275 vegetation species used for this isoprene EP update, a new map was created with leaf- and branch-level EFs. The new isoprene EP values were then converted to MEGANv2.1-suitable format. There is unfortunately no accurate conversion equation that would satisfy all conditions. A rough conversion can be made following recommendations by Arneth et al. (2011) and Messina et al. (2016) for conversion between the two systems. Details of the conversion of EMEP EFs to MEGANv2.1-suitable isoprene EPs are given in Sect. 2.5.2.

280 2.5.1 Land cover description and emission factors

The main basis for European BVOC emissions in Europe in the EMEP system is a map of forest species generated by Köble and Seufert (2001), combined with species-specific EFS for each of these species. The forest database provides maps for 115 tree species in 30 (mainly EU) European countries, based on a compilation of data from the ICP-forest network UN-ECE (1998). These data were further processed to the EMEP grid by the Stockholm Environment Institute at York (UK, S. Cinderby 285 pers. Comm., 2004) in order to add data from other countries in the (2000-era) EMEP domain, and for non-forested vegetation. More recently, the EMEP domain was significantly expanded to the east, and data for the expanded area and indeed globally makes use of a merge of the GLC_2000 dataset (<http://bioval.jrc.ec.europa.eu/products/glc2000/glc2000.php>) and data from the Community Land Model (<http://www.cgd.ucar.edu/models/clm/>, Oleson et al. 2010, Lawrence et al. 2011) as described in Simpson et al. (2017). In order to provide a manageable number of PFTs for use in MEGAN, tree species were aggregated in 290 six classes, as summarized in Table 3.



Table 3. Generic PFTs used for European emission potential maps based on EMEP.

PFT	Vegetation included	Examples	LAI variation	LAI max / m ² m ⁻²
CF	Temperate/boreal coniferous forest	norway spruce, scots pine	constant	5
DF	Temperate/boreal deciduous forest	european oak, beech, birch	variable	4
NF	Mediterranean needleleaf forest	cedars, eucalyptus, stone pine	constant	4
BF	Mediterranean broadleaf forest	holm oak, cork oak, arbutus	constant	4
SNL	Seminatural	moorland, tundra, shrub	variable	3
CR	Crops	all crops	variable	3.5

295 For each grid cell, the grid-average emission potential of a specific PFT (EP_{PFT} , $\mu\text{g m}^{-2} \text{h}^{-1}$) was then calculated as a weighted average of all the individual tree species belonging to this PFT category:

$$EP_{PFT} = \frac{\sum_i EF_i D_i A_i}{\sum_i A_i} \quad (3)$$

300 where i represents one of the many forest or vegetation species contained within that PFT, EF_i is the species foliage-level isoprene emission factor ($\mu\text{g g}(\text{dry leaf weight})^{-1} \text{h}^{-1}$), D_i is the species foliar density ($\text{g}(\text{dry leaf weight}) \text{m}^{-2}$) and A_i is the species area (m^2). Further details of this methodology, including detailed composition of each PFT class as well as EF and D values for each considered tree species can be found in Simpson et al. (2012) (Sect 6.6., SI, S4.4).

305 For the European-domain runs used here, the EMEP model combines the PFT-specific EPs and max-LAI, with latitude-dependent growing season dates as described in Simpson et al. (2012). For this work we have made use of much finer grid-resolution ($0.1^\circ \times 0.1^\circ$ latitude-longitude).

For non-forest vegetation types (e.g. grasslands, seminatural vegetation) or for forest areas not covered by the Köble and
 310 Seufert (2001) maps (e.g. for eastern Russia), default emission factors taken from Simpson et al. (2012) were applied.

The crops category is the most difficult to deal with in terms of BVOC emissions, not least because the types of crops are not well known (and can change significantly over the years), and the growing seasons almost impossible to specify. Here we used a simple system which defines the phenology and emission factors of crops using EMEP model definitions. For this study, the



315 EMEP model's temperate crop (wheat, etc.), Mediterranean crop (maize, etc.) and root-crop (potato, etc.) were aggregated into one Crop PFT.

The isoprene emission potential data (EP_{PFT}) and the monthly changes in LAI per each of the six PFTs were provided for a European domain spanning $[30.05^\circ - 71.95^\circ]$ in latitude and $[-29.95^\circ - 65.95^\circ]$ in longitude with $0.1^\circ \times 0.1^\circ$ spatial resolution.

320 2.5.2 Conversion of isoprene emission potential map for MEGAN

In order to satisfy the MEGANv2.1 definition of standard conditions, the EMEP-based isoprene emission potential maps needed to be converted. As discussed earlier, there is unfortunately no precise way of such conversion. According to recommendations of Arneth et al. (2011) and Messina et al. (2016) the following equation was used for conversion between the EMEP and MEGANv2.1 system.

325

MEGAN-suitable isoprene emission potentials EP_{MEGAN} ($\mu\text{g m}^{-2} \text{h}^{-1}$) were calculated for each month as:

$$EP_{MEGAN}[month] = LAI_{std} \frac{\sum_i^{PFT} f_i \frac{LAI_i[month]}{LAI_{max}} EP_{PFT i}}{\sum_i^{PFT} f_i LAI_i[month]} \quad (4)$$

330

where LAI_{std} is standard leaf area index in the MEGAN model equal to $5 \text{ m}^2 \text{ m}^{-2}$, i is an index through EMEP PFT categories (Table 3), f_i is a fraction of a grid cell covered by specific PFT, LAI and LAI_{max} are monthly and maximal leaf area index of the PFT category (see Table 3), respectively, and EP_{PFT} is EMEP-based isoprene emission potential for a specific PFT category.

335 Monthly isoprene emission potential maps for Europe were then embedded into the global domain of MEGAN gridded emission potential maps. These new global isoprene EPs were used in the calculation of the CAMS-GLOB-BIOv3.1 emission inventory.

3 Results and discussion

The following sections present examples of spatial and temporal distribution of emissions in CAMS-GLOB-BIO inventories on global and regional scales (Sect. 3.1 and 3.2). Section 3.3 focuses in more detail on the impact of land cover change on isoprene emissions and Section 3.4 on update of the isoprene emission potential data in Europe showing differences between emissions calculated with the MEGAN-default and updated input EP maps. Section 3.5 presents comparison of CAMS-GLOB-BIO isoprene and monoterpene emissions to other available datasets.



3.1 Global distribution of BVOC emissions

345 The annual global totals averaged over the respective periods are listed in Table 4 for BVOC species available in CAMS-
GLOB-BIOv1.2, v3.0 and v3.1 datasets. Though the absolute values differ between the datasets, the species responsible for
the majority of the global BVOC total are common to all three inventories. The most abundant species is isoprene (64 %),
followed by the sum of monoterpenes (13%), methanol (7%), acetone (4%), ethene (3.6%), sesquiterpenes (2.5%), propene
(2%), acetaldehyde (1.4%) and ethanol (1.3%). The numbers in brackets represent the species contribution to the global BVOC
350 total when expressed as Tg(C) yr⁻¹, averaged over the three datasets. The rest of species contribute together with less than 10
Tg(C) yr⁻¹, i.e. less than 2%. Note that for monoterpenes we provide emissions of α -pinene, β -pinene and other monoterpenes.
Other monoterpenes group is a sum of myrcene, sabinene, trans- β -ocimene, limonene and 2 Δ -carene, following
recommendations of Emmons et al. (2010).

355 The CAMS-GLOB-BIOv3.1 annual global total BVOC is about 60 Tg(C) yr⁻¹ higher than v1.2. This difference is mainly due
to use of different meteorological inputs. While v1.2 was calculated with ERA-Interim reanalysis, v3.1 is based on ERA5.
ERA-Interim data is available with 3 or 6 h time step and therefore to obtain hourly input fields for the MEGAN model, the
data needed to be temporally interpolated. Such interpolation leads to underestimation of meteorological parameters, especially
for air temperature and solar radiation, as the interpolated fields do not capture the noon peak hours at locations between the
360 model time steps. In the case of ERA5, the data are available with hourly timesteps and temporal interpolation is no longer
needed. The annual mean ERA5 values of air temperature and solar radiation are therefore higher than ERA-Interim, especially
in highly emitting regions of south America, central Africa, south-east Asia and Indonesia, which is reflected accordingly in
higher modeled emissions. Similar effects of temporal resolution of the input climate data on isoprene emissions were
discussed by e.g. Ashworth et al. (2010).

365
The largest difference in global emission total can be observed between the CAMS-GLOB-BIOv3.1 and v3.0 inventories. The
v3.0 emission total is more than 160 Tg(C) yr⁻¹ lower than in v3.1, with most significant difference for isoprene estimates
which are more than 140 Tg(isoprene) yr⁻¹ lower in v3.0 compared to v3.1. Both inventories are calculated with ERA5
meteorology, but they differ in setup of the input emission potential data and most importantly in the underlying land cover
370 description.

In the calculation of v3.0 we switched from using static CLM land cover maps to annually changing ESA-CCI land cover data
in order to capture the effect of land cover change on emissions. To include the effect of changing land cover information in
the model, input gridded emission potential maps (described in Sect 2.4.1) had to be replaced by calculation of emission
375 potentials from PFT distributions (described in Sect. 2.4.2). As discussed in Sect. 2.4.2, such a change in the model setup leads
to ~10% decrease of isoprene emissions on global scale. The rest of the isoprene decrease can be explained by different land



cover distribution in CLM and ESA-CCI datasets. Sensitivity emission model runs using exactly same input data except for definition of land cover distribution resulted in isoprene annual global total of 427 Tg(isoprene) yr⁻¹ when using CLM and 316 Tg(isoprene) yr⁻¹ when using ESA-CCI, i.e. almost 30 % difference. As shown in Table 1, total vegetated area is more than 18 million km² (19%) smaller in ESA-CCI than in CLM maps. Significant differences between the two vegetation maps are visible in the tropical region which is a source of ~80% of isoprene global emission (Guenther et al., 2012; Sindelarova et al., 2014). The extent of broadleaf evergreen and deciduous tree cover in ESA-CCI is about 25% lower than in CLM.

The global spatial distribution of CAMS-GLOB-BIOv3.1 emissions for selected species is presented in Fig. 1. Regions of highest emission are located in the tropical band and include Amazonia, central Africa south-east Asia, Indonesia and northern Australia.

Table 4. List of modeled NMVOC species with annual global emission totals (Tg(species) yr⁻¹) in CAMS-GLOB-BIOv3.1, v3.0 and v1.2 inventory averaged over the dataset period. Each species / group is assigned a molecular weight (right column) which was used to calculate total emissions in Tg(C) yr⁻¹.

species	CAMS-GLOB- BIO.v3.1	CAMS-GLOB- BIOv3.0	CAMS-GLOB- BIOv1.2	molecular weight
[Tg (species) yr ⁻¹]	2000 - 2019	2000 - 2019	2000 - 2017	[g mol ⁻¹]
isoprene	440.5	299.1	385.2	68
α-pinene	27.2	23.7	25.7	136
β-pinene	14.7	10.1	14.1	136
other monoterpenes	40.8	29.4	38.7	136
methanol	103.4	91.5	99.5	32
acetone	33.2	25.6	32.5	58
acetaldehyde	15.0	11.1	13.5	44
formaldehyde	3.7	2.9	3.4	30
propane	0.03	0.02	0.03	44
propene	13.3	10.9	13.0	40
ethane	0.28	0.23	0.27	30
ethene	23.5	19.2	21.9	28
ethanol	15.0	11.1	13.5	46
sesquiterpenes	16.6	11.9	14.9	204
toluene	1.2	1.0	1.1	92



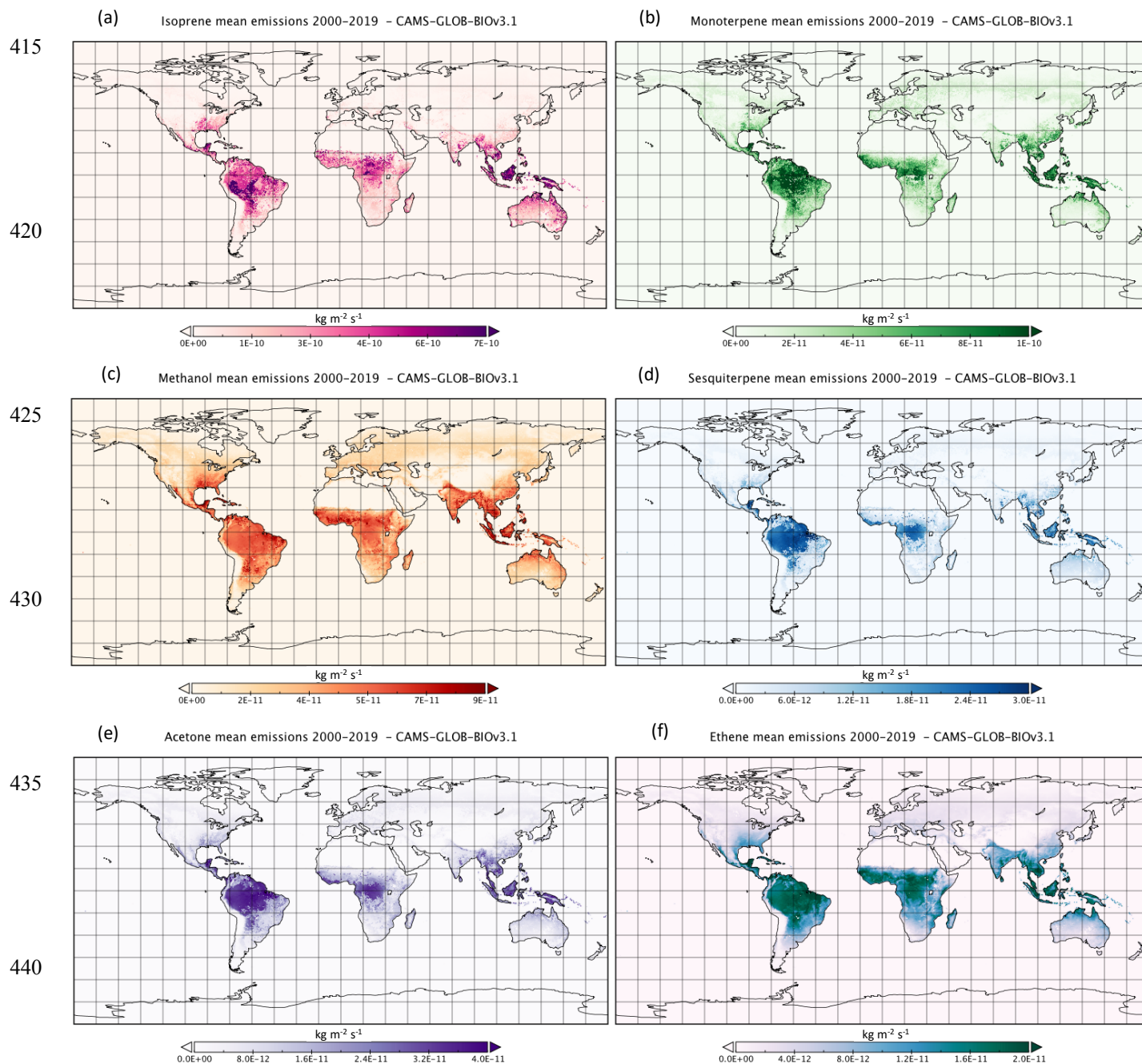
MBO	1.4	0.3	1.4	88
formic acid	2.8	2.2	2.5	46
acetic acid	2.8	2.2	2.5	60
butanes and higher alkanes	0.06	0.05	0.05	58
butenes and higher alkenes	2.7	2.2	2.6	56
other aldehydes	2.6	2.1	2.4	44
hydrogen cyanide	0.61	0.50	0.57	27
hydrogen sulfide	0.08	0.07	0.08	34
other ketones	0.6	0.5	0.6	72
total emissions				
<i>Tg (C) yr⁻¹</i>	591	424	532	
CO	71.2	58.1	65.3	28

395

400

405

410



445 **Figure 1: Spatial distribution of emissions averaged over the 2000–2019 period for (a) isoprene, (b) sum of monoterpenes, (c) methanol, (d) sum of sesquiterpenes, (e) acetone and (f) ethene in the CAMS-GLOB-BIOv3.1 dataset.**



450 Additionally, significant BVOC emission sources are located in the south-eastern part of the US, especially during the summer months of the northern hemisphere. Substantial amounts of monoterpenes and methanol are further emitted from the northern temperate and boreal forests. BVOC emissions have strong seasonal variation following local meteorological conditions and vegetation cycle with highest emissions during daytime and in summer season and lowest emissions during nighttime and winter months.

455 Temporals variation of isoprene, the most abundant BVOC species, for the period of 2000-2019 from CAMS-GLOB-BIOv3.1 dataset are presented in Fig. 2. The plot shows global monthly totals and interannual variation of emissions as well as isoprene zonal means. The zonal means stress again the tropical and southern subtropical band as the most important source of global isoprene with additional source in northern temperate latitudes.

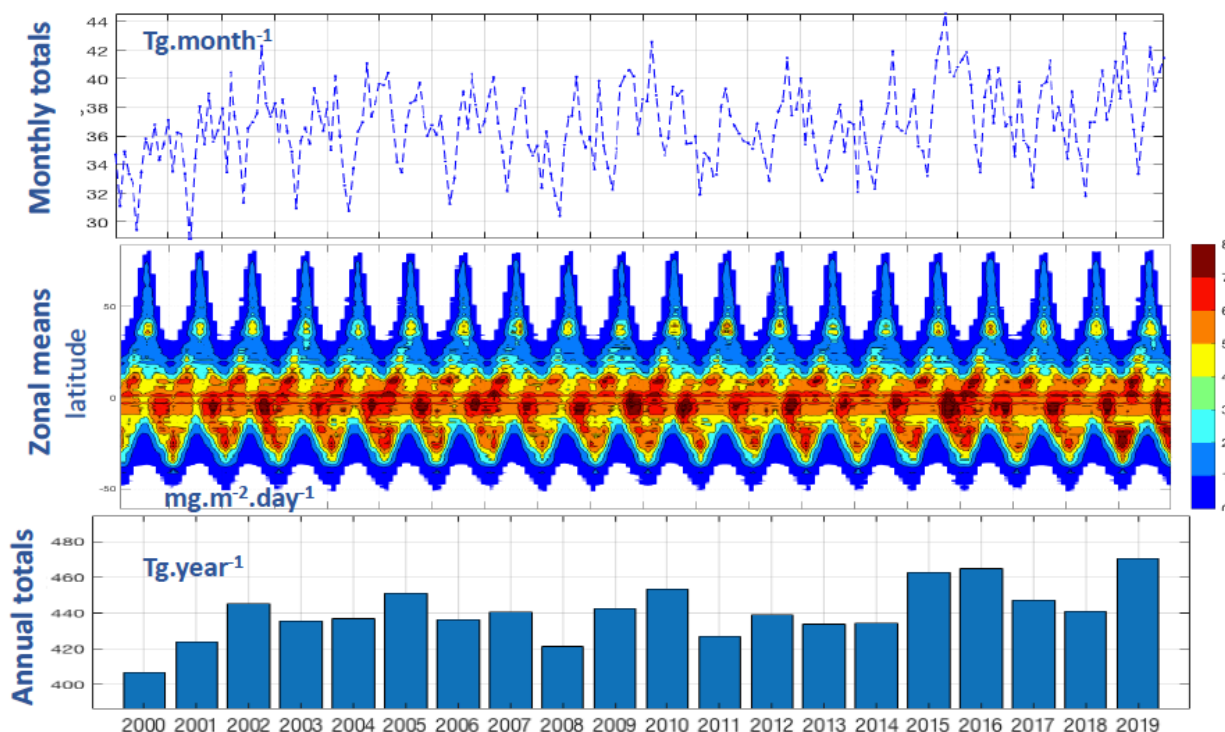
460 The interannual changes in emissions are driven partially by interannual changes in vegetation through changes in leaf area index, but to a greater extent by interannual changes in meteorology. There is a clear link between emissions and El Niño / La Niña phenomena. Annual global totals as well as zonal means in Fig. 2 show isoprene decrease in 2008 and 2011 when strong La Niña was identified and increase in 2002, 2015 and 2019 during El Niño episodes. Such a connection between BVOC emissions and El Niño phenomena was already noted in previous studies e.g. Naik et al. (2004), Müller et al. (2008) and in Wells et al. (2020).

465

470

475

480



485 **Figure 2: Global monthly totals (top), zonal means (middle) and global annual totals (bottom) of the isoprene emissions for the**
490 **period of 2000–2019 in the CAMS-GLOB-BIOv3.1 inventory.**

3.2 Regional distribution of emissions

The CAMS-GLOB-BIOv3.1 emissions of the main BVOC species for the year 2000 were further analyzed to show their regional contribution to global totals. We have used regions defined under the GlobEmission project
490 (<https://www.globemission.eu/>) which divide the globe to nine emitting areas. The spatial extent of the regions is given in Table 5 and shown in Fig. 3.

Table 5 presents the annual emission of isoprene, monoterpenes, methanol, acetone, sesquiterpenes and ethene from each of the regions together with their relative contribution to the global total. For all species (except for methanol), more than 70%
495 of emission originates in tropical regions of South America, East Africa and Southeast Asia and 10 – 18 % of emissions has its source in the northern latitudes (North America, Europe and Russia). Especially low, when compared to other species, is a production of isoprene in Europe and Russia, with less than 1% and 2 % of the global total, respectively. For methanol, the



tropics contribute with only 63% and almost 25% of methanol is produced in the northern latitudes, mainly in North America and Russia.

500

Table 5. Regional annual emissions for CAMS-GLOB-BIOv3.1 isoprene, monoterpenes, methanol, acetone, sesquiterpenes and ethene expressed as $Tg(species) yr^{-1}$ and as a percentage of the global total.

region	Latitude extent	Longitude extent	Regional annual emissions [$Tg(species) yr^{-1}$ % of global total]					
	[latmin - latmax]	[lonmin - lonmax]	isoprene	monoterpenes	methanol	acetone	sesquiterpenes	ethene
North America	13°N - 75°N	40°E - 170°E	31 8%	7 9%	12 12%	3 10%	1.2 8%	2.1 9.5%
South America	60°S - 13°N	35°E - 90°E	133 33%	27 34%	23 24%	10 33%	6 39%	6 29%
Europe	36°N - 75°N	50°W - 15°E	3.6 0.9%	2.8 4%	5 5%	1.1 3%	0.2 1.3%	0.7 3%
N. Af. + Mid. East	15°N - 37°N	65°W - 20°E	6 1.4%	0.5 0.6%	1.4 1.4%	0.3 0.9%	0.1 0.7%	0.3 1.4%
East Africa	15°S - 15°N	55°W - 20°E	93 23%	15 19.5%	20 21%	6.5 21%	3 21%	5 24%
South Africa	15°S - 35°S	55°W - 20°E	13 3%	2.5 3%	4 4%	1 3%	0.3 2%	1 4.5%
Russia	37°N - 75°N	50°W - 179°W	7 1.8%	4 5%	7 7%	1.5 5%	0.4 2.7%	1 4.5%
Southeast Asia	10°S - 37°N	65°W - 170°W	74 18%	15 19%	18 18.5%	6 18%	3 18.7%	4 18%
Australia	10°S - 50°S	65°W - 179°W	46 11%	4 5.5%	7 7%	2 6%	1 6.7%	1.4 6%
Globe	89°S - 89°N	179°E - 179°W	407	78	97	32	15	22

505

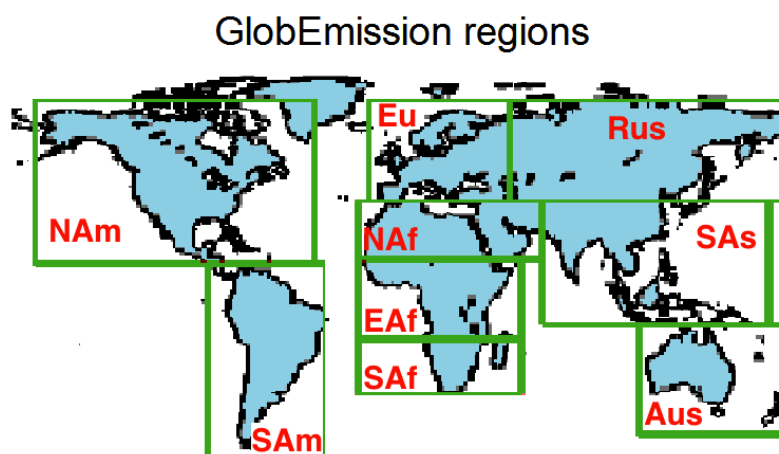


Figure 3: Geographical extent of the GlobEmission regions. Adapted from GlobEmission (<https://www.globemission.eu/>).



3.3 Impact of land cover change on isoprene emissions

510 The impact of changing land cover on emissions is captured in the CAMS-GLOB-BIOv3.0 dataset. To illustrate the effect of
changing land cover on isoprene, the 20-year time series of isoprene annual totals was fitted with linear regression trend and
compared to data from v3.1 for which a static CLM land cover map was used. When calculated with static vegetation map,
isoprene emissions increase globally by 0.35 % yr⁻¹ due to temporal changes in meteorology. When annually changing ESA-
CCI data are implemented, the trend decreases to 0.24 % yr⁻¹. Similar observation was made by Opacka et al. (2021), who
515 used a modified MODIS land cover data in the MEGAN-MOHYCAN emission model to study the impact of land cover change
on isoprene emissions. They found a 0.04 to 0.33 % yr⁻¹ mitigating effect of land cover change on general positive trends of
isoprene induced mainly by temperature and solar radiation.

Figure 4 presents a comparison of the v3.0 and v3.1 isoprene emission trends in selected regions. The regions' definition and
520 spatial extent is given in Table 5. Inclusion of land cover change through ESA-CCI data (v3.0) reduces isoprene trends in
South America (esp. in the Amazon) or even causes a negative isoprene trend in Southeast Asia when compared to v3.1 based
on static land cover. Such trend decline is caused mainly by retreat of tropical broadleaf forest (broadleaf evergreen and
deciduous trees) in these locations. On the other hand, we observe an increase to isoprene trend in East Africa, North Africa +
Middle East and Russia where the ESA-CCI data show an increase of broadleaf deciduous tree category (tropical and boreal)
525 in the course of the 20-year period. Moderate decrease to isoprene trend (relative difference of -20 to -30%) can be observed
in North America, South Africa and Australia and the trend remains almost unchanged between the v3.0 and v3.1 data in
Europe.

530

535

540

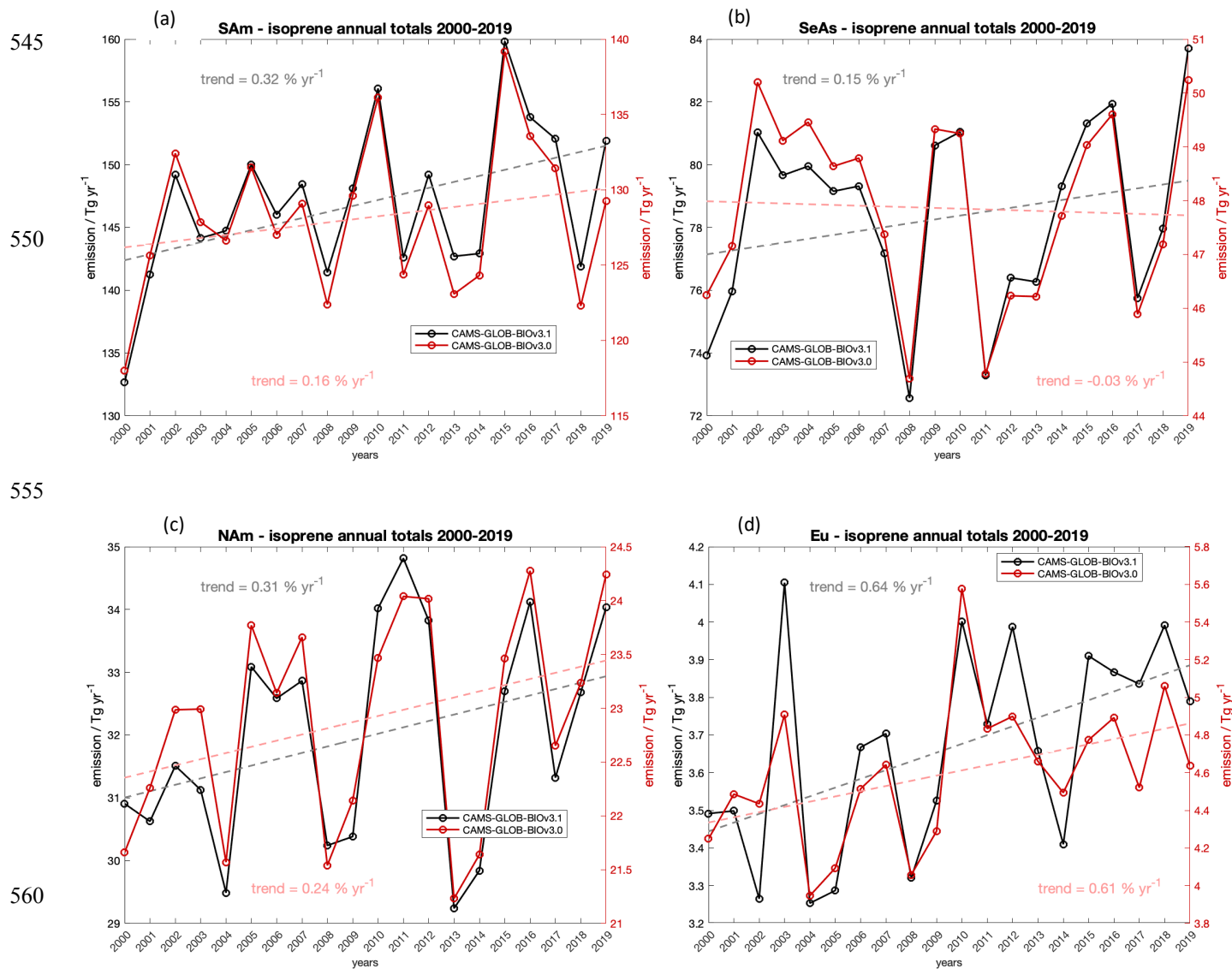


Figure 4: Comparison of isoprene annual totals from CAMS-GLOB-BIOv3.0 and v3.1 in (a) South America, (b) Southeast Asia and Indonesia, (c) North America and (d) Europe with linear trend for each dataset (dashed line and trend value in [$\% \text{ yr}^{-1}$]).

3.4 Isoprene emission update in Europe

Updated isoprene emission potential values in Europe, to more detail described in Sect. 2.5, were used to calculate isoprene emissions in CAMS-GLOB-BIOv3.1. Spatial distribution of annual mean isoprene emissions in Europe is presented in Fig. 5,



where CAMS-GLOB-BIOv3.1 emissions are compared with emissions obtained directly from the EMEP model (v4.33, Simpson et al., 2019) and with isoprene emissions calculated with MEGAN and v3.1 similar settings (i.e. meteorology, PFT distribution, LAI), but using the MEGAN-default emission potential maps instead of the updated EPs.

Figure 5 shows a good agreement in spatial distribution and amount of calculated emissions between the EMEP and v3.1 emissions which approves the approach of updated EP calculation and conversion from EMEP inputs to MEGAN format. It can also be seen that the spatial distribution of isoprene emissions changes when updated EPs are applied. Emissions calculated with MEGAN-default EPs are more uniformly distributed over the European domain, while v3.1 emissions are more localized, with isoprene hotspots in areas covered by highly-emitting tree species, e.g. in Portugal, Spain, southern France, and Balkan peninsula.

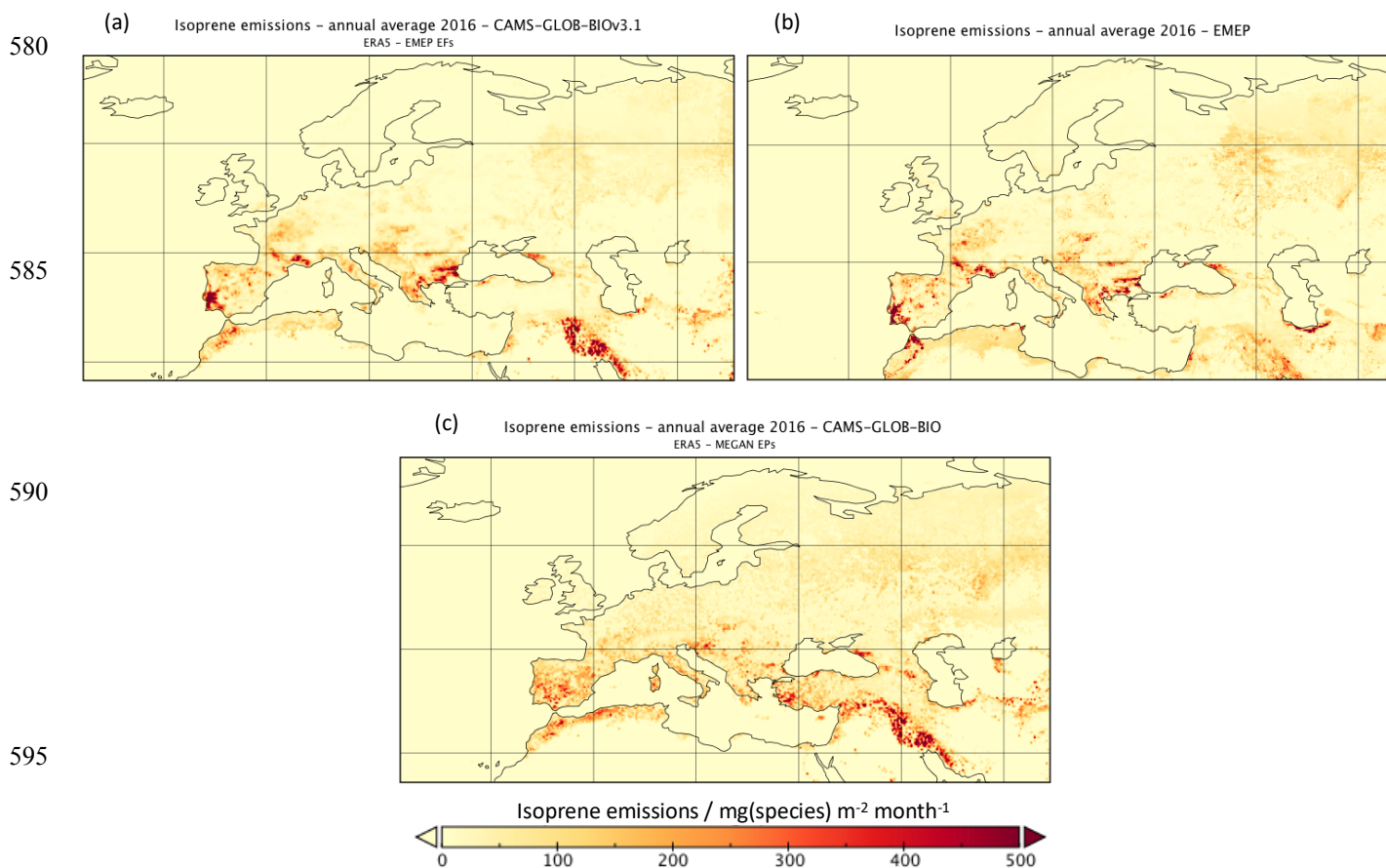
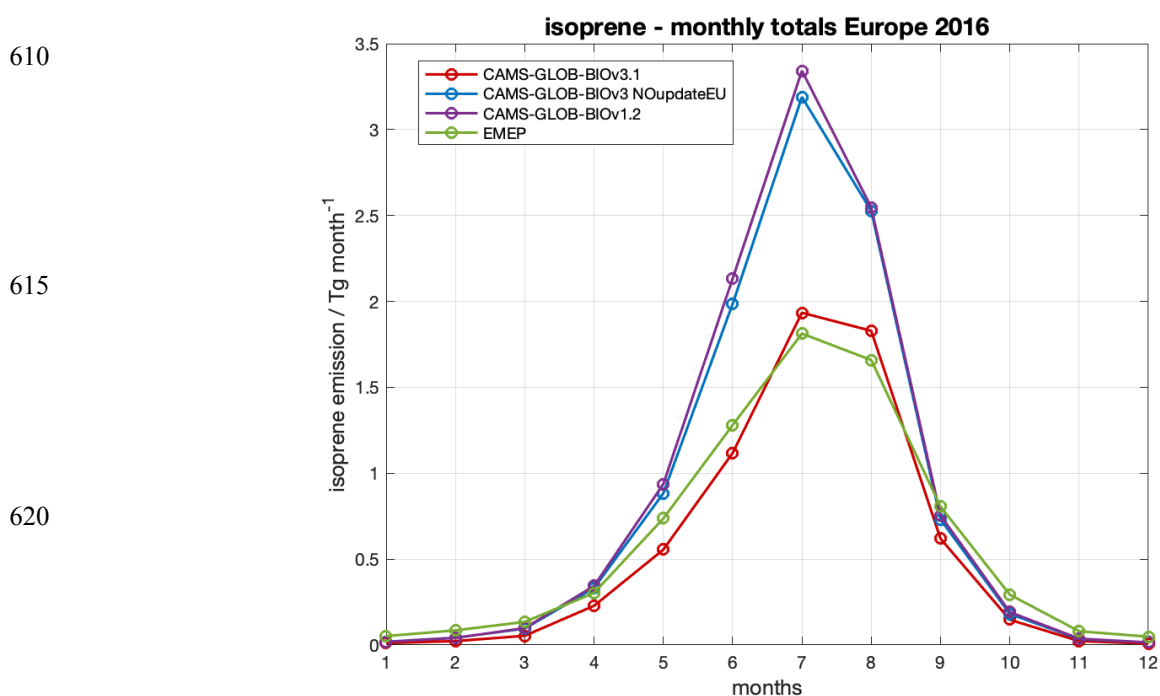


Figure 5: Comparison of European annual mean isoprene emissions in 2016 from (a) the EMEP model and (b) CAMS-GLOB-BIOv3.1. Bottom panel (c) shows annual mean isoprene emissions calculated with default MEGAN EP maps.



Use of updated instead of MEGAN-default EPs in Europe leads to 35% decrease of isoprene annual total from 10.03 Tg yr⁻¹ (v3.1 without EP update) to 6.55 Tg yr⁻¹ (v3.1). Isoprene monthly totals from these two datasets are compared to CAMS-GLOB-BIOv1.2 (annual total of 10.5 Tg yr⁻¹) and to isoprene estimated by EMEP (7.3 Tg yr⁻¹) in Fig 6. The plot shows a clear decrease of emissions after use of the updated EPs and a good agreement between the CAMS-GLOB-BIOv3.1 and EMEP estimates. The results were extracted for the European domain with latitude from 30.5° to 71.75°, longitude from -29.75° to 65.75°.



625 **Figure 6: Isoprene monthly totals in Europe in year 2016 from CAMS-GLOB-BIO datasets (v3.1, v3.1 without EP update and v1.2) and EMEP model.**

3.5 Comparison of CAMS-GLOB-BIO emissions with other inventories

Time series of CAMS-GLOB-BIO emissions of isoprene and monoterpenes were compared to other available data. We focus on isoprene and monoterpenes as these are the two most abundant BVOC species and the two species for which time series from other sources are available. The rest of the species unfortunately suffers from lack of available and time-varying data.

Datasets gathered for this comparison are listed in Table 6. Each dataset is assigned with basic information such as model used for emission estimation and driving meteorology. Most of the inventories are so called ‘bottom-up’, i.e. modeled by an



emission model based on meteorology, emission factors and vegetation distribution. There are two ‘top-down’ datasets, IASB-
 635 TD-OMI and IASB-TD-GOME2, which were calculated by an emission model and then constrained with satellite observations
 of formaldehyde (from OMI and GOME2) by applying an inversion technique in chemical transport model (IMAGESv2)
 (Stavrakou et al., 2014, 2015). Most of the inventories were calculated with ‘MEGAN-like’ emission model algorithm. Except
 for the GUESS dataset, which was estimated by a process-based model LPJ-GUESS (Smith et al., 2001; Sitch et al., 2003).
 The IASB datasets were obtained from website of the GlobEmission project (<http://www.globemission.eu/>). The rest of the
 640 data were obtained from the ECCAD database (<http://eccad.aeris-data.fr/>).

Table 6. List of datasets used for comparison of emissions.

<i>dataset</i>	<i>period</i>	<i>model</i>	<i>meteorology</i>	<i>inversion</i>	<i>reference</i>
CAMS-GLOB-BIOv3.1	2000-2019	MEGANv2.1	ERA5	-	This paper
CAMS-GLOB-BIOv3.0	2000-2019	MEGANv2.1	ERA5	-	This paper
CAMS-GLOB-BIO.v1.2	2000-2017	MEGANv2.1	ERA-Interim	-	This paper
MEGAN-MACC	1980-2017	MEGANv2.1	MERRA/MERRA2	-	Sindelarova et al. (2014)
IASB-TD-OMI	2005-2014	MEGAN-MOHYCAN	ERA-Interim	OMI	Stavrakou et al. (2015)
IASB-TD-GOME2	2007-2012	MEGAN-MOHYCAN	ERA-Interim	GOME2	Stavrakou et al. (2014)
IASB-BU-OMI	2005-2014	MEGAN-MOHYCAN	ERA-Interim	-	Stavrakou et al. (2015)
GUESS	2000-2009	LPJ-GUESS	CRU	-	Arneeth et al. (2007a)
MEGANv2	2003	MEGANv2.0	NCEP	-	Guenther et al. (2006)

645
 Figures 7 and 8 show a comparison of isoprene and monoterpene annual totals within the 2000 – 2019 period, respectively. In
 both cases, the CAMS-GLOB-BIO emissions fall well within the range of other estimates. Though both plots show there is
 quite a large spread between the datasets with maximal differences up to factor of 2 to 3 (difference of 320 Tg yr⁻¹ for isoprene
 and 61 Tg yr⁻¹ for monoterpenes). There are various reasons for these discrepancies, with the most important being selection
 650 of the emission model, driving meteorology and input vegetation data (land cover description and emission factors).

In this data collection, the highest isoprene and monoterpene emissions are estimated by the MEGAN-MACC dataset. This
 dataset was calculated based on the MERRA/MERRA2 reanalyzes (Rienecker et al., 2011) and therefore differs in the use of
 meteorological inputs from most of the remaining datasets which used ERA meteorological fields (ERA-Interim and ERA5).
 655 Comparison of 2 m temperature and PAR fields from MERRA and ERA datasets showed higher values of both meteorological
 parameters in the MERRA dataset mainly in the tropical regions of South America, central Africa and Australia, i.e. locations



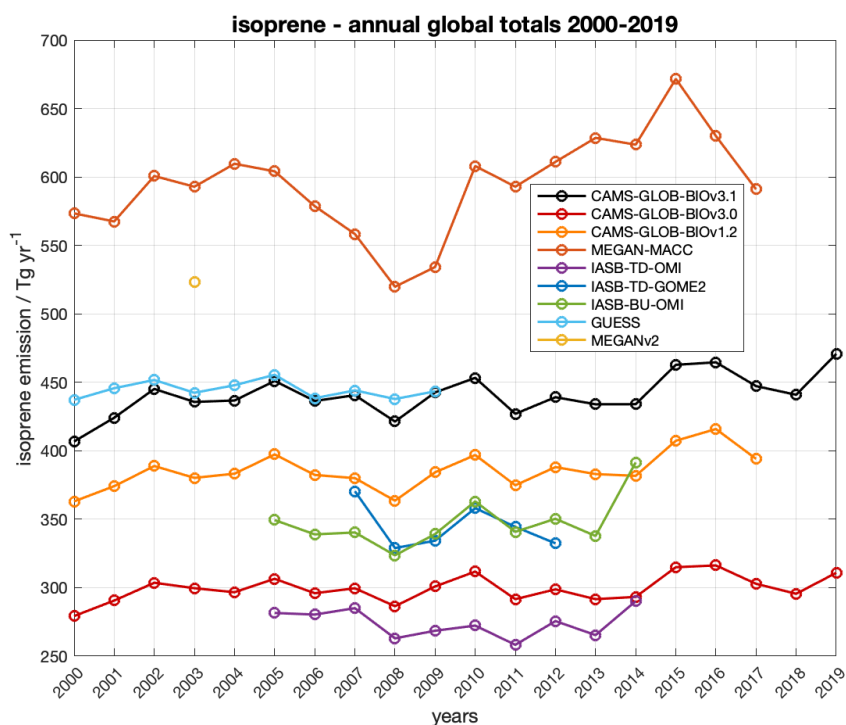
of high BVOC emission potential. Higher temperature and PAR values in MERRA data then reflects in higher MEGAN-MACC estimates.

660 The key role of meteorology in BVOC estimation is supported also by a relatively good agreement of CAMS-GLOB-BIOv1.2 isoprene emissions with IASB datasets, esp. IASB-BU-OMI and IASB-TD-GOME2, which are both calculated based on ERA-Interim fields. Furthermore, the impact of meteorological inputs can be also observed in the difference between CAMS-GLOB-BIOv1.2 and v3.1 estimates, based on ERA-Interim and ERA5, respectively, which was already discussed in Sect. 3.1.

665 Inter-annual variability for most of the datasets is similar as they are mostly driven by the ERA meteorology. Again, except for MEGAN-MACC based on MERRA reanalysis for which the amplitude is higher. For all datasets there is a clear link between isoprene emissions and El Niño / La Niña phenomena. As also presented in Fig. 2, isoprene emissions decrease in 2008 and 2011 during strong La Niña and increase in 2002, 2015 and 2019 during El Niño episodes.

670 For monoterpenes the inter-annual variability is not as profound as for isoprene. Similar to isoprene, monoterpenes are strongly emitted in the tropical region. But have also significant sources in the temperate and boreal forests in the northern hemisphere. As a result, they are not as susceptible to atmospheric changes in the tropical band as isoprene and keep rather stable inter-annual profile.

675



680

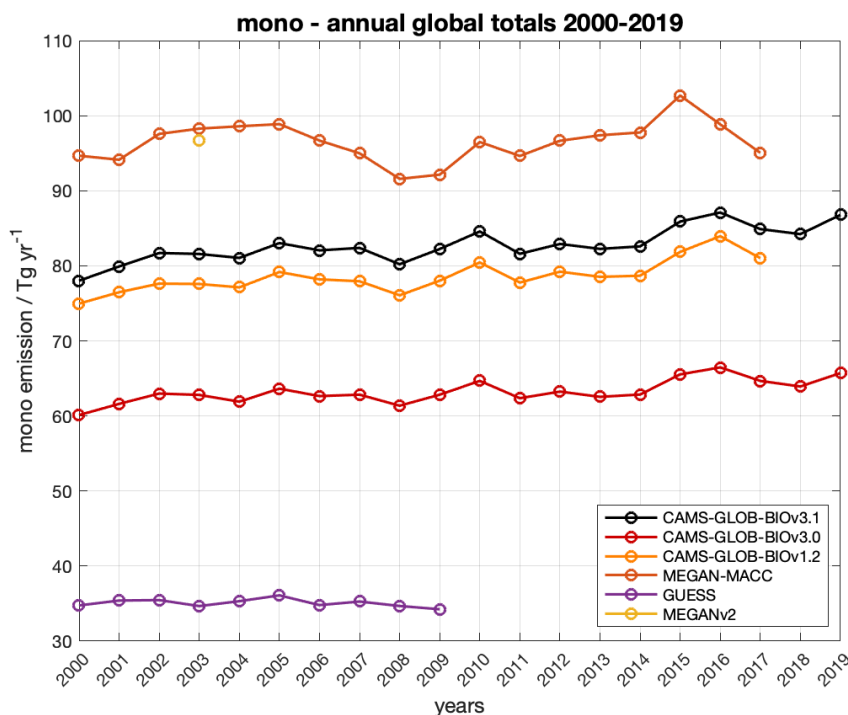
685



690

Figure 7: Comparison of isoprene global annual totals from CAMS-GLOB-BIOv3.1 (in black), CAMS-GLOB-BIOv3.0 (red), CAMS-GLOB-BIOv1.2 (orange) and other available inventories within the 2000–2019 period.

695



700

705

710

Figure 8: Comparison of monoterpene global annual totals from CAMS-GLOB-BIOv3.1 (black), CAMS-GLOB-BIOv3.0 (red), CAMS-GLOB-BIOv1.2 (orange) and other available inventories within the 2000–2019 period.

715 4 Data availability

Gridded maps with global emissions per species available as monthly means or monthly averaged daily profiles are provided as NetCDF (Network Common Data Format) files for the global domain at a resolution of $0.5^\circ \times 0.5^\circ$ (CAMS-GLOB-BIOv1.2, <https://doi.org/10.24380/t53a-qw03>, Sindelarova et al., 2021a), and at a resolution of $0.25^\circ \times 0.25^\circ$ (CAMS-GLOB-BIOv3.0, <https://doi.org/10.24380/xs64-gj42>, Sindelarova et al., 2021b; CAMS-GLOB-BIOv3.1, <https://doi.org/10.24380/cv4p-5f79>, Sindelarova et al., 2021c) and can be accessed through the Emissions of atmospheric Compounds and Compilation of Ancillary Data (ECCAD) system with a login account (<https://eccad.aeris-data.fr/>, last access: June 2021). For review purposes, ECCAD

720



has set up an anonymous repository where subsets of the CAMS-GLOB-BIOv1.2, CAMS-GLOB-BIOv3.0 and CAMS-GLOB-BIOv3.1 data can be accessed directly (<https://eccad.aeris-data.fr/essd-surf-emis-cams-bio/>, last access: June 2021).

5 Conclusions

725 The presented paper describes three new global inventories of biogenic volatile organic compounds emitted from vegetation which are publicly available for use by the air quality and climate models. The datasets are called CAMS-GLOB-BIO v1.2, v3.0 and v3.1, and were calculated with the Model of Emissions of Gases and Aerosols from Nature (MEGANv2.1) driven by meteorological reanalyzes of the European Centre for Medium-Range Weather Forecasts (ECMWF). Inventories include emissions of 25 BVOC species or chemical groups provided as monthly means and monthly averaged daily profiles spanning
730 through the period of 2000–2019. The CAMS-GLOB-BIO datasets were developed under the Copernicus Atmosphere Monitoring Service project (CAMS, Global and Regional Emissions) as part of the European Union’s Copernicus Earth Observation Programme.

The dataset CAMS-GLOB-BIOv1.2 is based on ERA-Interim meteorological fields and is available with horizontal spatial
735 resolution of $0.5^\circ \times 0.5^\circ$. Datasets CAMS-GLOB-BIOv3.1 and v3.0 were calculated with ERA5 meteorology and are provided with horizontal spatial resolution of $0.25^\circ \times 0.25^\circ$.

The CAMS-GLOB-BIOv3.1 estimates global annual total BVOC emission of $591 \text{ Tg(C) yr}^{-1}$ with isoprene as the main contributing species ($440.5 \text{ Tg(isoprene) yr}^{-1}$). Use of ERA5 meteorology in v3.1 leads to a slight increase of BVOC emissions
740 compared to v1.2 with global BVOC total of $532 \text{ Tg(C) yr}^{-1}$ (including $385.2 \text{ Tg(isoprene) yr}^{-1}$). The total emission in CAMS-GLOB-BIOv3.0 dataset is $424 \text{ Tg(C) yr}^{-1}$ with isoprene emissions of $299.1 \text{ Tg(isoprene) yr}^{-1}$. The difference between v3.1 and v3.0 estimates can mostly be attributed to use of an alternative land cover map for vegetation description.

The CAMS-GLOB-BIOv3.1 include isoprene estimates in Europe calculated with updated map of emission potential values
745 which are based on fine-scale land cover with detailed maps of tree species, and should therefore better represent the composition of European forests than the global EP maps of the MEGAN model. Use of updated isoprene EP maps led to a substantial decrease of European isoprene emission total by 35% and caused a change in spatial distribution of emissions. Isoprene emissions are concentrated in several emission hot spots in locations covered by highly-emitting tree species.

750 Both v3.1 and v1.2 estimates are based on a static land cover description obtained from the Community Land Model (CLM4). Since the world’s vegetation is experiencing significant changes, such as deforestation in the tropical region, replacement of forests by agricultural land, afforestation efforts with fast-growing trees, we aimed to take this effect into account. Dataset CAMS-GLOB-BIOv3.0 considers changes in global land cover by using the ESA-CCI annual land cover maps for vegetation



description in the MEGAN model. In order to use a new land cover input in the model, the emission potentials had to be
755 calculated from the PFT distribution instead of using the high-resolution emission potential maps. Such difference in input EP
data and different input land cover map (ESA-CCI instead of CLM4) caused a decrease of ~30% for annual total isoprene and
~ 20% for monoterpenes when compared to CAMS-GLOB-BIOv3.1. The linear trend analysis of the 20-year time series of
global isoprene emissions showed that inclusion of time-varying land cover data causes a decrease in general isoprene growing
760 trend from 0.35 % yr⁻¹ to 0.24 % yr⁻¹. The trend slowdown is even more profound in the tropical regions of South America and
Southeast Asia, where according to ESA-CCI data the retreat of tropical broadleaf forest can be observed. On the other hand,
due to expansion of broadleaf deciduous trees the isoprene increasing trend is intensified in regions such as East and Central
Africa or Russia.

Time series of CAMS-GLOB-BIO isoprene and monoterpene emissions were compared to other available data. The estimates
765 fall well within the range of values from other studies. Though the comparison shows there is quite large uncertainty in
emission estimates which on global scale can reach up to factor of 2 to 3, with even higher values on regional level. The
different emission estimates in different versions of the CAMS-GLOB-BIO datasets suggest the uncertainty main driving
factors, i.e. meteorological inputs, definition of input emission potentials and land cover distribution.

770 The presented CAMS-GLOB-BIO datasets provide a high-resolution data of global BVOC emissions for the period of 20
recent years based on up-to-date input data. The datasets are suitable for the purposes of air quality modelling, especially for
models that do not include their own module for online BVOC emission estimation. Our general recommendation is to use a
CAMS-GLOB-BIO dataset which is calculated with the same meteorology as drives the air quality model. If this does not
apply, we recommend using the latest CAMS-GLOB-BIOv3.1 dataset. CAMS-GLOB-BIOv3.0 should be used for studies
775 focusing on land cover change.

Author contribution

KS performed the emission model runs, created emission inventories and analyzed the data, JM contributed to preparation of
model inputs and emission processing, DS provided data for the update of isoprene emission potentials in Europe, helped with
its conversion to MEGAN model format and analysis of emissions, PH and JK participated on emission modelling, SD and
780 CG performed the emission data formatting and upload to the emission database. KS wrote the manuscript with contributions
from all co-authors.



Acknowledgements

The research leading to these results has received funding from the Copernicus Atmosphere Monitoring Service (CAMS), which is implemented by the European Centre for Medium-Range Weather Forecasts (ECMWF) on behalf of the European Commission. The project was coordinated by the Centre National de la Recherche Scientifique (CNRS, Claire Granier) and by the TNO (Hugo Denier van der Gon).

References

- Arnth, A., Miller, P. A., Scholze, M., Hickler, T., Schurgers, G., Smith, B., and Prentice, I. C.: CO₂ inhibition of global terrestrial isoprene emissions: Potential implications for atmospheric chemistry, *Geophys. Res. Lett.*, 34, L18813, doi:10.1029/2007GL030615, 2007a.
- Arnth, A., Niinemets, Ü., Pressley, S., Bäck, J., Hari, P., Karl, T., Noe, S., Prentice, I. C., Serça, D., Hickler, T., Wolf, A., and Smith, B.: Process-based estimates of terrestrial ecosystem isoprene emissions: incorporating the effects of a direct CO₂-isoprene interaction, *Atmos. Chem. Phys.*, 7, 31–53, <https://doi.org/10.5194/acp-7-31-2007>, 2007b.
- Arnth, A., Schurgers, G., Lathiere, J., Duhl, T., Beerling, D. J., Hewitt, C. N., Martin, M., and Guenther, A.: Global terrestrial isoprene emission models: sensitivity to variability in climate and vegetation, *Atmos. Chem. Phys.*, 11, 8037-8052, <https://doi.org/10.5194/acp-11-8037-2011>, 2011.
- Ashworth, K., Wild, O., and Hewitt, C. N.: Sensitivity of isoprene emissions estimated using MEGAN to the time resolution of input climate data, *Atmos. Chem. Phys.*, 10, 1193–1201, <https://doi.org/10.5194/acp-10-1193-2010>, 2010.
- Atkinson, R. and Arey, J.: Gas-phase tropospheric chemistry of biogenic volatile organic compounds: a review, *Atmos. Environ.*, 37, 197–219, 2003.
- Bauwens, M., Stavrou, T., Müller, J.-F., De Smedt, I., Van Roozendael, M., van der Werf, G. R., Wiedinmyer, C., Kaiser, J. W., Sindelarova, K., and Guenther, A.: Nine years of global hydrocarbon emissions based on source inversion of OMI formaldehyde observations, *Atmos. Chem. Phys.*, 16, 10133–10158, <https://doi.org/10.5194/acp-16-10133-2016>, 2016.
- Curci, G., Beekman, M., Vautard, R., Smiatek, G., and Steinbrecher, R.: Modelling study of the impact of isoprene and terpene biogenic emissions on European ozone levels, *Atmos. Environ.*, 43, 1444–1455, 2009.



Curci, G., Palmer, P. I., Kurosu, T. P., Chance, K., and Visconti, G.: Estimating European volatile organic compound emissions using satellite observations of formaldehyde from the Ozone Monitoring Instrument, *Atmos. Chem. Phys.*, 10, 11501–11517, 815 <https://doi.org/10.5194/acp-10-11501-2010>, 2010.

Dee, D. P., Uppala, S. M., Simmons, A. J., Berrisford, P., Poli, P., Kobayashi, S., Andrae, U., Balmaseda, M. A., Balsamo, G., Bauer, P., Bechtold, P., Beljaars, A. C. M., van de Berg, L., Bidlot, J., Bormann, N., Delsol, C., Dragani, R., Fuentes, M., Geer, A. J., Haimberger, L., Healy, S. B., Hersbach, H., Hólm, E. V., Isaksen, L., Kållberg, P., Köhler, M., Matricardi, M., 820 McNally, A. P., Monge-Sanz, B. M., Morcrette, J.-J., Park, B.-K., Peubey, C., de Rosnay, P., Tavolato, C., Thépaut, J.-N. and Vitart, F.: The ERA-Interim reanalysis: configuration and performance of the data assimilation system. *Q.J.R. Meteorol. Soc.*, 137: 553–597. doi: [10.1002/qj.828](https://doi.org/10.1002/qj.828), 2011.

Eerdeken, G., Ganzeveld, L., Vilà-Guerau de Arellano, J., Klüpfel, T., Sinha, V., Yassaa, N., Williams, J., Harder, H., 825 Kubistin, D., Martinez, M., and Lelieveld, J.: Flux estimates of isoprene, methanol and acetone from airborne PTR-MS measurements over the tropical rainforest during the GABRIEL 2005 campaign, *Atmos. Chem. Phys.*, 9, 4207–4227, <https://doi.org/10.5194/acp-9-4207-2009>, 2009.

Ehn, M., Thornton, J. A., Kleist, E., Sipila, M., Junninen, H., Pullinen, I., Springer, M., Rubach, F., Tillmann, R., Lee, B., 830 Lopez-Hilfiker, F., Andres, S., Acir, I.-H., Rissanen, M., Jokinen, T., Schobesberger, S., Kangasluoma, J., Kontkanen, J., Nieminen, T., Kurten, T., Nielsen, L. B., Jorgensen, S., Kjaergaard, H. G., Canagaratna, M., Maso, M. D., Berndt, T., Petaja, T., Wahner, A., Kerminen, V.-M., Kulmala, M., Worsnop, D. R., Wildt, J., and Mentel, T. F.: A large source of low-volatility secondary organic aerosol, *Nature*, 506, 476–479, <http://dx.doi.org/10.1038/nature13032>, 2014.

835 Emmerson, K. M., Cope, M. E., Galbally, I. E., Lee, S., and Nelson, P. F.: Isoprene and monoterpene emissions in south-east Australia: comparison of a multi-layer canopy model with MEGAN and with atmospheric observations, *Atmos. Chem. Phys.*, 18, 7539–7556, <https://doi.org/10.5194/acp-18-7539-2018>, 2018.

Emmons, L. K., Walters, S., Hess, P. G., Lamarque, J.-F., Pfister, G. G., Fillmore, D., Granier, C., Guenther, A., Kinnison, D., 840 Laepple, T., Orlando, J., Tie, X., Tyndall, G., Wiedinmyer, C., Baughcum, S. L., and Kloster, S.: Description and evaluation of the Model for Ozone and Related chemical Tracers, version 4 (MOZART-4), *Geosci. Model Dev.*, 3, 43–67, <https://doi.org/10.5194/gmd-3-43-2010>, 2010.

ESA. Land Cover CCI Product User Guide Version 2. Tech. Rep. (2017). Available at:
845 maps.elie.ucl.ac.be/CCI/viewer/download/ESACCI-LC-Ph2-PUGv2_2.0.pdf, access date 31/5/2021, 2017.



- Escobedo, J.F., Gomes, E.N., Oliveira, A.P., and Soares, J.: Ratios of UV, PAR and NIR components to global solar radiation measured at Botucatu site in Brazil, *Renewable Energy*, 36, 169 – 178, doi:10.1016/j.renene.2010.06.018, 2011.
- 850 Fares, S., Mereu, S., Scarascia Mugnozza, G., Vitale, M., Manes, F., Frattoni, M., Ciccio, P., Gerosa, G., and Loreto, F.: The ACCENT-VOCBAS field campaign on biosphere-atmosphere interactions in a Mediterranean ecosystem of Castelporziano (Rome): site characteristics, climatic and meteorological conditions, and eco-physiology of vegetation, *Biogeosciences*, 6, 1043–1058, <https://doi.org/10.5194/bg-6-1043-2009>, 2009.
- 855 Fu, D., Millet, D.B., Wells, K.C., Payne, V.H., Yu, S., Guenther, A. and Eldering, A.: Direct retrieval of isoprene from satellite-based infrared measurements, *Nature Communications* 10, 3811, <https://doi.org/10.1038/s41467-019-11835-0>, 2019.
- Gelencsér, A., May, B., Simpson, D., Sánchez-Ochoa, A., Kasper-Giebl, A., Puxbaum, H., Caseiro, A., Pio, C., and Legrand, M.: Source apportionment of PM_{2.5} organic aerosol over Europe: primary/secondary, natural/anthropogenic, fossil/biogenic
860 origin, *J. Geophys. Res.*, 112, D23S04, <https://doi.org/10.1029/2006JD008094>, 2007.
- Griffin, R. J., David R, C. I., Seinfeld, J. H., and Dabdub, D.: Estimate of global atmospheric organic aerosol from oxidation of biogenic hydrocarbons, *Geophys. Res. Lett.*, 26, 2721–2724, 1999.
- 865 Guenther, A., Hewitt, C. N., Erickson, D., Fall, R., Geron, C., Graedel, T., Harley, P., Klinger, L., Lerdau, M., McKay, W. A., Pierce, T., Scholes, B., Steinbrecher, R., Tallamraju, R., Taylor, J., and Zimmerman, P.: A global model of natural volatile organic compound emissions, *J. Geophys. Res.*, 100, 8873–8892, 1995.
- Guenther, A., Karl, T., Harley, P., Wiedinmyer, C., Palmer, P. I., and Geron, C.: Estimates of global terrestrial isoprene
870 emissions using MEGAN (Model of Emissions of Gases and Aerosols from Nature), *Atmos. Chem. Phys.*, 6, 3181–3210, doi:10.5194/acp-6-3181-2006, 2006.
- Guenther, A. B., Jiang, X., Heald, C. L., Sakulyanontvittaya, T., Duhl, T., Emmons, L. K., and Wang, X.: The Model of Emissions of Gases and Aerosols from Nature version 2.1 (MEGAN2.1): an extended and updated framework for modeling
875 biogenic emission, *Geosci. Model Dev.*, 5, 1471–1492, doi:10.5194/gmd-5-1471-2012, 2012.
- Hantson, S., Knorr, W., Schurgers, G., Pugh, T.A.M. and Arneth, A.: Global isoprene and monoterpene emissions under changing climate, vegetation, CO₂ and land use, *Atmospheric Environment*, Volume 155, p. 35-45, <https://doi.org/10.1016/j.atmosenv.2017.02.010>, 2017.



- Hao, L. Q., Romakkaniemi, S., Yli-Pirilä, P., Joutsensaari, J., Kortelainen, A., Kroll, J. H., Miettinen, P., Vaattovaara, P., Tiitta, P., Jaatinen, A., Kajos, M. K., Holopainen, J. K., Heijari, J., Rinne, J., Kulmala, M., Worsnop, D. R., Smith, J. N., and Laaksonen, A.: Mass yields of secondary organic aerosols from the oxidation of α -pinene and real plant emissions, *Atmos. Chem. Phys.*, 11, 1367–1378, <https://doi.org/10.5194/acp-11-1367-2011>, 2011.
- 885
- Heald, C. L., Henze, D. K., Horowitz, L. W., Feddema, J., Lamarque, J.-F., Guenther, A., Hess, P. G., Vitt, F., Seinfeld, J. H., Goldstein, A. H., and Fung, I.: Predicted change in global secondary organic aerosol concentrations in response to future climate, emissions, and land use change, *J. Geophys. Res.-Atmos.*, 113, D05211, doi:10.1029/2007JD009092, 2008.
- 890
- Heald, C. L., Wilkinson, M. J., Monson, R. K., Alo, C. A., Wang, G., and Guenther, A.: Response of isoprene emission to ambient CO₂ changes and implications for global budgets, *Global Change Biol.*, 15, 1127–1140, 2009.
- Henrot, A.-J., Stanelle, T., Schröder, S., Siegenthaler, C., Taraborrelli, D., and Schultz, M. G.: Implementation of the MEGAN (v2.1) biogenic emission model in the ECHAM6-HAMMOZ chemistry climate model, *Geosci. Model Dev.*, 10, 903-926, <https://doi.org/10.5194/gmd-10-903-2017>, 2017.
- 895
- Hersbach, H., Bell, B., Berrisford, P., Hirahara, S., Horányi, A., Muñoz-Sabater, J., Nicolas, J., Peubey, C., Radu, R., Schepers, D., Simmons, A., Soci, C., Abdalla, S., Abellan, X., Balsamo, G., Bechtold, P., Biavati, G., Bidlot, J., Bonavita, M., De Chiara, G., Dahlgren, P., Dee, D., Dimantakis, M., Dragani, R., Flemming, J., Forbes, R., Fuentes, M., Geer, A., Haimberger, L., 900 Healy, S., Hogan, R.J., Hólm, E., Janisková, M., Keeley, S., Lalovaux, P., Lopez, P., Lupu, C., Radnoti, G., de Rosnay, P., Rozum, I., Vamborg, F., Villaume, S. and Thépaut, J.-N.: The ERA5 global reanalysis, *Quarterly Journal of the Royal Meteorological Society*, Vol. 146, Issue 730, p. 1999-2049, doi: <https://doi.org/10.1002/qj.3803>, 2020.
- Hewitt, C.N., Karl, T., Langford, B., Owen, S.M. and Possel, M.: Quantification of VOC emission rates from biosphere, *Trends in Analytical Chemistry*, Vol. 30, No 7., doi:10.1016/j.trac.2011.03.008, 2011.
- 905
- Hodzic, A., Jimenez, J. L., Prevot, A. S. H., Szidat, S., Fast, J. D., and Madronich, S.: Can 3-D models explain the observed fractions of fossil and non-fossil carbon in and near Mexico City?, *Atmos. Chem. Physics*, 10, 10 997–11 016, <https://doi.org/10.5194/acp-10-10997-2010>, 2010.
- 910
- Houweling, S., Dentener, F., and Lelieveld, J.: The impact of nonmethane hydrocarbon compounds on tropospheric photochemistry, *J. Geophys. Res.*, 103, 10673–10696, 1998.



Jacovides, C.P., Tymvios, F.S., Asimakopoulos, D.N., Theofilou, K.M., and Pashiardes, S.: Global photosynthetically active
915 radiation and its relationship with global solar radiation in the Eastern Mediterranean basin, *Theor. Appl. Climatol.*, 74, 227 –
233, DOI 10.1007/s00704-002-0685-5, 2003.

Huszár, P., Karlický, J., Belda, M., Halenka, T. and Pišoft, P.: [The impact of urban canopy meteorological forcing on summer
photochemistry](https://doi.org/10.1016/j.atmosenv.2017.12.037), *Atmos. Environ.*, 176, 209-228, <https://doi.org/10.1016/j.atmosenv.2017.12.037>, 2018.

920

Huszar, P., Karlický, J., Ďoubalová, J., Nováková, T., Šindelářová, K., Švábik, F., Belda, M., Halenka, T., and Žák, M.: The
impact of urban land-surface on extreme air pollution over central Europe, *Atmos. Chem. Phys.*, 20, 11655–11681,
<https://doi.org/10.5194/acp-20-11655-2020>, 2020.

925 Jiang, J., Aksoyoglu, S., Ciarelli, G., Oikonomakis, E., El-Haddad, I., Canonaco, F., O'Dowd, C., Ovadnevaite, J., Minguillón,
M. C., Baltensperger, U., and Prévôt, A. S. H.: Effects of two different biogenic emission models on modelled ozone and
aerosol concentrations in Europe, *Atmos. Chem. Physics*, 19, 3747–3768, doi:10.5194/acp-19-3747-2019, URL
<https://www.atmos-chem-phys.net/19/3747/2019/>, 2019.

930 Kaiser, J., Jacob, D. J., Zhu, L., Travis, K. R., Fisher, J. A., González Abad, G., Zhang, L., Zhang, X., Fried, A., Crouse, J.
D., St. Clair, J. M., and Wisthaler, A.: High-resolution inversion of OMI formaldehyde columns to quantify isoprene emission
on ecosystem-relevant scales: application to the southeast US, *Atmos. Chem. Phys.*, 18, 5483–5497,
<https://doi.org/10.5194/acp-18-5483-2018>, 2018.

935 Karl, T., Guenther, A., Yokelson, R. J., Greenberg, J., Potosnak, M., Blake, D. R., and Artaxo, P.: The tropical forest and fire
emissions experiment: emission, chemistry, and transport of biogenic volatile organic compounds in the lower atmosphere
over Amazonia, *J. Geophys. Res.*, 112, D18302, doi:10.1029/2007JD008539, 2007.

Karl, M., Guenther, A., Köble, R., Leip, A., and Seufert, G.: A new European plant-specific emission inventory of biogenic
940 volatile organic compounds for use in atmospheric transport models, *Biogeosciences*, 6, 1059–1087,
<https://doi.org/10.5194/bg-6-1059-2009>, 2009.

Keller, C. A., Long, M. S., Yantosca, R. M., Da Silva, A. M., Pawson, S., and Jacob, D. J.: HEMCO v1.0: a versatile, ESMF-
compliant component for calculating emissions in atmospheric models, *Geosci. Model Dev.*, 7, 1409-1417,
945 <https://doi.org/10.5194/gmd-7-1409-2014>, 2014.



Kesselmeier, J. and Staudt, M.: Biogenic Volatile Organic Compounds (VOC): an overview on emission, physiology and ecology, *J. Atmos. Chem.*, 33, 23–88, 1999.

950 Köble, R. and Seufert, G.: Novel Maps for Forest Tree Species in Europe., in: *A Changing Atmosphere*, 8th European Symposium on the Physico-Chemical Behaviour of Atmospheric Pollutants, Torino, Italy, 17-20 Sept., 2001.

Kuhn, U., Andreae, M. O., Ammann, C., Araújo, A. C., Brancaleoni, E., Ciccioli, P., Dindorf, T., Frattoni, M., Gatti, L. V., Ganzeveld, L., Kruijt, B., Lelieveld, J., Lloyd, J., Meixner, F. X., Nobre, A. D., Pöschl, U., Spirig, C., Stefani, P., Thielmann,
955 A., Valentini, R., and Kesselmeier, J.: Isoprene and monoterpene fluxes from Central Amazonian rainforest inferred from towerbased and airborne measurements, and implications on the atmospheric chemistry and the local carbon budget, *Atmos. Chem. Phys.*, 7, 2855–2879, doi:10.5194/acp-7-2855-2007, 2007.

Langford, B., Misztal, P. K., Nemitz, E., Davison, B., Helfter, C., Pugh, T. A. M., MacKenzie, A. R., Lim, S. F., and Hewitt,
960 C. N.: Fluxes and concentrations of volatile organic compounds from a South-East Asian tropical rainforest, *Atmos. Chem. Phys.*, 10, 8391–8412, doi:10.5194/acp-10-8391-2010, 2010.

Langner, J., Engardt, M., Baklanov, A., Christensen, J. H., Gauss, M., Geels, C., Hedegaard, G. B., Nuterman, R., Simpson, D., Soares, J., Sofiev, M., Wind, P., and Zakey, A.: A multi-model study of impacts of climate change on surface ozone in
965 Europe, *Atmos. Chem. Physics*, 12, 10 423–10 440, doi:10.5194/acp-12-10423-2012, URL <http://www.atmos-chem-phys.net/12/10423/2012/>, 2012.

Lathière, J., Hauglustaine, D.A. and De Noblet-Ducoudré, N.: Past and future changes in biogenic volatile organic compound emissions simulated with a global dynamic vegetation model, *Geophysical Research Letters*, Vol. 32, L20818,
970 doi:10.1029/2005GL024164, 2005.

Lathière, J., Hauglustaine, D. A., Friend, A. D., De Noblet-Ducoudré, N., Viovy, N., and Folberth, G. A.: Impact of climate variability and land use changes on global biogenic volatile organic compound emissions, *Atmos. Chem. Phys.*, 6, 2129–2146,
doi:10.5194/acp-6-2129-2006, 2006.

975

Lawrence, P. J. and Chase, T. N.: Representing a new MODIS consistent land surface in the Community Land Model (CLM 3.0), *J. Geophys. Res.-Biogeo.*, 112, G01023, doi:10.1029/2006JG000168, 2007.

Lawrence, D. M., Oleson, K. W., Flanner, M. G., Thornton, P. E., Swenson, S. C., Lawrence, P. J., Zeng, X., Yang, Z.-L.,
980 Levis, S., Sakaguchi, K., Bonan, G. B. and Slater, A. G.: Parameterization improvements and functional and structural



- advances in version 4 of the Community Land Model, *J. Adv. Model. Earth Syst.*, 3, M03001, doi:10.1029/2011MS000045, 2011.
- 985 Lemire, K., Allen, D., Klouda, G., and Lewis, C.: Fine Particulate Matter Source Attribution for Southeast Texas using $^{14}\text{C}/^{13}\text{C}$ Ratios, *J. Geophys. Res.*, 107, <https://doi.org/10.1029/2002JD002339>, 2002.
- Lowe, P.R. and J.M. Ficke: The computation of saturation vapor pressure. Tech.Paper No. 4-74, Environmental Prediction Research Facility, Naval Postgraduate School, Monterey, CA, 1974.
- 990 Messina, P., Lathière, J., Sindelarova, K., Vuichard, N., Granier, C., Ghattas, J., Cozic, A., and Hauglustaine, D. A.: Global biogenic volatile organic compound emissions in the ORCHIDEE and MEGAN models and sensitivity to key parameters, *Atmos. Chem. Phys.*, 16, 14169–14202, <https://doi.org/10.5194/acp-16-14169-2016>, 2016.
- 995 McFiggans, G., Mentel, T. F., Wildt, J., Pullinen, I., Kang, S., Kleist, E., Schmitt, S., Springer, M., Tillmann, R., Wu, C., Zhao, D., Hallquist, M., Faxon, C., Le Breton, M., Hallquist, A. M., Simpson, D., Bergstroem, R., Jenkin, M. E., Ehn, M., Thornton, J. A., Alfarra, M. R., Bannan, T. J., Percival, C. J., Priestley, M., Topping, D., and Kiendler-Scharr, A.: Secondary organic aerosol reduced by mixture of atmospheric vapours, *Nature*, 565, 587–593, <https://doi.org/10.1038/s41586-018-0871-y>, <https://doi.org/10.1038/s41586-018-0871-y>, 2019.
- 1000 Millet, D. B., Jacob, D. J., Boersma, K. F., Fu, T.-M., Kurosu, T. P., Chance, K., Heald, C. L., and Guenther, A.: Spatial distribution of isoprene emissions from North America derived from formaldehyde column measurements by the OMI satellite sensor, *J. Geophys. Res.-Atmos.*, 113, D02307, doi:10.1029/2007JD008950, 2008.
- 1005 Misztal, P. K., Nemitz, E., Langford, B., Di Marco, C. F., Phillips, G. J., Hewitt, C. N., MacKenzie, A. R., Owen, S. M., Fowler, D., Heal, M. R., and Cape, J. N.: Direct ecosystem fluxes of volatile organic compounds from oil palms in South-East Asia, *Atmos. Chem. Phys.*, 11, 8995–9017, <https://doi.org/10.5194/acp-11-8995-2011>, 2011.
- 1010 Müller, J.-F., Stavrou, T., Wallens, S., De Smedt, I., Van Roozendaal, M., Potosnak, M. J., Rinne, J., Munger, B., Goldstein, A., and Guenther, A. B.: Global isoprene emissions estimated using MEGAN, ECMWF analyses and a detailed canopy environment model, *Atmos. Chem. Phys.*, 8, 1329–1341, doi:10.5194/acp-8-1329-2008, 2008.
- Naik, V., Delire, C., and Wuebbles, D. J.: Sensitivity of global biogenic isoprenoid emissions to climate variability and atmospheric CO_2 , *J. Geophys. Res.-Atmos.*, 109, D06301, doi:10.1029/2003JD004236, 2004.



1015

Oderbolz, D. C., Aksoyoglu, S., Keller, J., Barmpadimos, I., Steinbrecher, R., Skjøth, C. A., Plaß-Dülmer, C., and Prévôt, A. S. H.: A comprehensive emission inventory of biogenic volatile organic compounds in Europe: improved seasonality and land-cover, *Atmos. Chem. Phys.*, 13, 1689-1712, <https://doi.org/10.5194/acp-13-1689-2013>, 2013.

1020

Olofsson, P., Van Laake, P.E. and Eklundh, L.: Estimation of absorbed PAR across Scandinavia from satellite measurements Part I: Incident PAR, *Remote Sensing of Environment*, 110, 252 - 261, doi:10.1016/j.rse.2007.02.021, 2007.

Opacka, B., Müller, J.-F., Stavrakou, T., Bauwens, M., Sindelarova, K., Markova, J., and Guenther, A. B.: Global and regional impacts of land cover changes on isoprene emissions derived from spaceborne data and the MEGAN model, *Atmos. Chem.*

1025

Phys., 21, 8413–8436, <https://doi.org/10.5194/acp-21-8413-2021>, 2021.

Pacifico, F., Harrison, S. P., Jones, C. D., Arneth, A., Sitch, S., Weedon, G. P., Barkley, M. P., Palmer, P. I., Serça, D., Potosnak, M., Fu, T.-M., Goldstein, A., Bai, J., and Schurgers, G.: Evaluation of a photosynthesis-based biogenic isoprene emission scheme in JULES and simulation of isoprene emissions under presentday climate conditions, *Atmos. Chem. Phys.*, 11, 4371–

1030

4389, doi:10.5194/acp-11-4371-2011, 2011.

Palmer, P.I., Abbot, D.S., Fu, T.-M., Jacob, D.J., Chance, K., Kurosu, T.P., Guenther, A., Wiedinmyer, C., Stanton, J.C., Pilling, M.J., Pressley, S.N., Lamb, B. and Sumner, A.L.: Quantifying the seasonal and interannual variability of North American isoprene emissions using satellite observations of the formaldehyde column, *Journal of Geophysical Research*, Vol.

1035

111, D12315, doi:10.1029/2005JD006689, 2006.

Pfister, G., Emmons, L., Hess, P., Lamarque, J.-F., Orlando, J., Walters, S., Guenther, A., Palmer, P., and Lawrence, P.: Contribution of isoprene to chemical budgets: a model tracer study with the NCAR CTM MOZART-4, *J. Geophys. Res.-Atmos.*, 113, D05308, doi:10.1029/2007JD008948, 2008.

1040

Poisson, N., Kanakidou, M., and Crutzen, P. J.: Impact of nonmethane hydrocarbons on tropospheric chemistry and the oxidizing power of the global troposphere: 3-dimensional modelling results, *J. Atmos. Chem.*, 36, 157–230, 2000.

Poulter, B., MacBean, N., Hartley, A., Khlystova, I., Arino, O., Betts, R., Bontemps, S., Boettcher, M., Brockmann C., Defourny, P., Hagemann, S., Herold, M., Kirches, G., Lamarche, C., Lederer, D., Otlé, C., Peters, M., and Peylin, P.: Plant functional type classification for earth system models: results from the European Space Agency's Land Cover Climate Change Initiative, *Geosci. Model Dev.*, 8, 2315–2328, <https://doi.org/10.5194/gmd-8-2315-2015>, 2015.

1045



- Rienecker, M. M., Suarez, M. J., Gelaro, R., Todling, R., Bacmeister, J., Liu, E., Bosilovich, M. G., Schubert, S. D., Takacs,
1050 L., Kim, G.-K., Bloom, S., Junye, C., Collins, D., Conaty, A., da Silva, A., Gu, W., Joiner, J., Koster, R. D., Lucchesi, R.,
Molod, A., Owens, T., Pawson, S., Pegion, P., Redder, C. R., Reichle, R., Robertson, F. R., Ruddick, A. G., Sienkiewicz, M.,
and Woollen, J.: MERRA: NASA's modern-era retrospective analysis for research and applications, *J. Climate*, 24, 3624–
3648, 2011.
- 1055 Rinne, H. J. I., Guenther, A. B., Greenberg, J. P., and Harely, P., C.: Isoprene and monoterpene fluxes measured above
Amazonian rainforest and their dependence on light and temperature, *Atmos. Environ.*, 36, 2421–2426, 2002.
- Rinne, J., Back, J., and Hakola, H.: Biogenic volatile organic compound emissions from the Eurasian taiga: current knowledge
and future directions, *Boreal Env. Res.*, 14, 807–826, 2009.
- 1060 Sanderson, M.G., Jones, C.D., Collins, W.J., Johnson C.E. and Derwent, R.G.: Effect of Climate Change on Isoprene
Emissions and Surface Ozone Levels, *Geophysical Research Letters*, Vol. 30, No. 18, 1936, doi:10.1029/2003GL017642,
2003.
- 1065 Sartelet, K. N., Couvidat, F., Seigneur, C., and Roustan, Y.: Impact of biogenic emissions on air quality over Europe and North
America, *Atmos. Environ.*, 53, 131–141, 2012.
- Schurgers, G., Arneth, A., Holzinger, R., and Goldstein, A. H.: Process-based modelling of biogenic monoterpene emissions
combining production and release from storage, *Atmos. Chem. Phys.*, 9, 3409–3423, <https://doi.org/10.5194/acp-9-3409-2009>,
1070 2009.
- Seco, R., Karl, T., Guenther, A., Hosman, K. P., Pallardy, S. G., Gu, L., Geron, C., Harley, P., and Kim, S.: Ecosystem scale
volatile organic compound fluxes during an extreme drought in a broadleaf temperate forest of the Missouri Ozarks (central
USA), *Glob. Change Biol.*, 21, 3657–3674, 2015.
- 1075 Simpson, D., Guenther, A., Hewitt, C. and Steinbrecher, R., Biogenic emissions in Europe 1. Estimates and uncertainties, *J.*
Geophys. Res., 100, 22875-22890, 1995.
- Simpson, D., Winiwarter, W., Borjesson, G. et al., Inventorying emissions from Nature in Europe, *J. Geophys. Res.*, 104,
1080 8113-8152, 1999.



- 1085 Simpson, D., Yttri, K., Klimont, Z., Kupiainen, K., Caseiro, A., Gelencsér, A., Pio, C., and Legrand, M.: Modeling Carbonaceous Aerosol over Europe. Analysis of the CARBOSOL and EMEP EC/OC campaigns, *J. Geophys. Res.*, 112, D23S14, <https://doi.org/10.1029/2006JD008158>, 2007.
- 1090 Simpson, D., Benedictow, A., Berge, H., Bergström, R., Emberson, L. D., Fagerli, H., Flechard, C. R., Hayman, G. D., Gauss, M., Jonson, J. E., Jenkin, M. E., Nyíri, A., Richter, C., Semeena, V. S., Tsyro, S., Tuovinen, J.-P., Valdebenito, A., and Wind, P.: The EMEP MSC-W chemical transport model – technical description, *Atmos. Chem. Physics*, 12, 7825–7865, doi:10.5194/acp-12-7825-2012, URL <http://www.atmos-chem-phys.net/12/7825/2012/acp-12-7825-2012.html>, 2012.
- 1095 Simpson, D., Bergström, R., Imhof, H., and Wind, P.: Updates to the EMEP/MSC-W model, 2016–2017, in: Transboundary particulate matter, photo-oxidants, acidifying and eutrophying components. Status Report 1/2017, pp. 115–122, The Norwegian Meteorological Institute, Oslo, Norway, www.emep.int, 2017.
- 1100 Simpson, D., Bergström, R., Tsyro, S., and Wind, P.: Updates to the EMEP/MSC-W model, 2018–2019, in: Transboundary particulate matter, photo-oxidants, acidifying and eutrophying components. EMEP Status Report 1/2019, pp. 145–155, The Norwegian Meteorological Institute, Oslo, Norway, 2019.
- 1105 Sindelarova, K., Granier, C., Bouarar, I., Guenther, A., Tilmes, S., Stavrou, T., Müller, J.-F., Kuhn, U., Stefani, P., and Knorr, W.: Global data set of biogenic VOC emissions calculated by the MEGAN model over the last 30 years, *Atmos. Chem. Phys.*, 14, 9317–9341, <https://doi.org/10.5194/acp-14-9317-2014>, 2014.
- 1110 Sindelarova, K., Markova, J., Simpson, D., Huszar, P., Karlicky, J., Darras, S., Granier, C.: Copernicus Atmosphere Monitoring Service Global Biogenic VOC emissions version 1.2 (CAMSGLOB-BIOv1.2), Copernicus Atmosphere Monitoring Service, ECCAD, <https://doi.org/10.24380/t53a-qw03>, 2021a.
- 1110 Sindelarova, K., Markova, J., Simpson, D., Huszar, P., Karlicky, J., Darras, S., Granier, C.: Copernicus Atmosphere Monitoring Service Global Biogenic VOC emissions version 3.0 (CAMSGLOB-BIOv3.0), Copernicus Atmosphere Monitoring Service, ECCAD, <https://doi.org/10.24380/xs64-gj42>, 2021b.
- 1110 Sindelarova, K., Markova, J., Simpson, D., Huszar, P., Karlicky, J., Darras, S., Granier, C.: Copernicus Atmosphere Monitoring Service Global Biogenic VOC emissions version 3.1 (CAMSGLOB-BIOv3.1), Copernicus Atmosphere Monitoring Service, ECCAD, <https://doi.org/10.24380/cv4p-5f79>, 2021c.



- 1115 Sitch, S., Smith, B., Prentice, I. C., Arneth, A., Bondeau, A., Cramer, W., Kaplan, J., Levis, S., Lucht, W., Sykes, M., Thonicke, K. and Venevsky, S.: Evaluation of ecosystem dynamics, plant geography and terrestrial carbon cycling in the LPJ dynamic global vegetation model, *Global Change Biol.*, 9, 161–185, 2003.
- Situ, S., Guenther, A., Wang, X., Jiang, X., Turnipseed, A., Wu, Z., Bai, J., and Wang, X.: Impacts of seasonal and regional
1120 variability in biogenic VOC emissions on surface ozone in the Pearl River delta region, China, *Atmos. Chem. Phys.*, 13, 11803–11817, <https://doi.org/10.5194/acp-13-11803-2013>, 2013.
- Smith, B., Prentice, I. C., and Sykes, M. T.: Representation of vegetation dynamics in the modelling of terrestrial ecosystems: comparing two contrasting approaches within European climate space, *Global. Ecol. Biogeogr.*, 10, 621–637, 2001.
- 1125 Song, XP., Hansen, M.C., Stehman, S.V., Potapov, P.V., Tvukavina, A., Vermote, E.F. and Townshend, J.R.: Global land change from 1982 to 2016. *Nature* **560**, 639–643, <https://doi.org/10.1038/s41586-018-0411-9>, 2018.
- Stavrou, T., Müller, J.-F., De Smedt, I., Van Roozendaal, M., van der Werf, G. R., Giglio, L., and Guenther, A.: Global
1130 emissions of non-methane hydrocarbons deduced from SCIAMACHY formaldehyde columns through 2003–2006, *Atmos. Chem. Phys.*, 9, 3663–3679, doi:10.5194/acp-9-3663-2009, 2009.
- Stavrou, T., J.-F. Müller, M. Bauwens, I. De Smedt, M. Van Roozendaal, A. Guenther, M. Wild, and X. Xia, Isoprene
emissions over Asia 1979–2011: impact of climate and land use changes, *Atmos. Chem. Phys.*, 14, 4587–4605, 2014.
- 1135 Stavrou, T., J.-F. Müller, M. Bauwens, I. De Smedt, M. Van Roozendaal, M. De Mazière, C. Vigouroux, F. Hendrick, M. George, C. Clearbaux, P.-F. Coheur, and A. Guenther, How consistent are top-down hydrocarbon emissions based on formaldehyde observations from GOME-2 and OMI? *Atmos. Chem. Phys.*, 15, 12007–12067, doi:10.5194/acpd-15-12007-2015, 2015.
- 1140 Steinbrecher, R., Smiatek, G., Köble, R., Seufert, G., Theloke, J., Hauff, K., Ciccioli, P., Vauratd, R., and Curci, G.: Intra- and inter-annual variability of VOC emissions from natural and seminatural vegetation in Europe and neighbouring countries, *Atmos. Environ.*, 43, 1380–1391, 2009.
- 1145 Tagaris, E., Sotiropoulou, R.E.P., Gounaris, N., Andronopoulos, S. and Vlachogiannis, D.: Impact of biogenic emissions on ozone and fine particles over Europe: Comparing effects of temperature increase and a potential anthropogenic NO_x emissions abatement strategy, *Atmospheric Environment*, Volume 98, p. 214–223, <https://doi.org/10.1016/j.atmosenv.2014.08.056>, 2014.



1150 UN-ECE: International Co-operative Programme on Assessment and Monitoring of Air Pollution Effects on Forests. Manual
on methods and criteria for harmonized sampling, assessment, monitoring and analysis of the effects of air pollution on forests.
(<http://icp-forests.net>), 1998.

van Donkelaar, A., Martin, R. V., Park, R. J., Heald, C. L., Tzung- May Fu, Hong Liao, and Guenther, A.: Model evidence for
1155 a significant source of secondary organic aerosol from isoprene, *Atmos. Environ.*, 41, 1267–1274, 2007.

Wells, K.C., Millet, D.B., Payne, V.H., Deventer, M.J., Bates, K.H., de Gouw, J.A., Graus, M., Warneke, C., Wisthaler, A.
and Fuenther, J.D.: Satellite isoprene retrievals constrain emissions and atmospheric oxidation, *Nature* 585, 225–233,
<https://doi.org/10.1038/s41586-020-2664-3>, 2020.

1160

Williams, J. E., van Velthoven, P. F. J., and Brenninkmeijer, C. A. M.: Quantifying the uncertainty in simulating global
tropospheric composition due to the variability in global emission estimates of Biogenic Volatile Organic Compounds, *Atmos.*
Chem. Phys., 13, 2857–2891, <https://doi.org/10.5194/acp-13-2857-2013>, 2013.

1165 Wu, K., Yang, X., Chen, D., Gu, S., Lu, Y., Jiang, Q., Wang, K., Ou, Y., Qian, Y., Shao, P. and Lu, S.: Estimation of biogenic
VOC emissions and their corresponding impact on ozone and secondary organic aerosol formation in China, *Atmospheric*
Research, Volume 231, 104656, <https://doi.org/10.1016/j.atmosres.2019>, 2020.

Yuan, H., Dai, Y., Xiao, Z., Ji, D., and Shanguan, W.: Reprocessing the MODIS Leaf Area Index products for land surface
1170 and climate modelling, *Remote Sens. Environ.*, 115, 1171–1187, 2011.